CFD MODELING OF PLASMA THERMAL REACTOR FOR WASTE TREATMENT

A Thesis

Submitted to the Faculty

of

Purdue University

by

Sikandar Y. Mashayak

In Partial Fulfillment of the

Requirements for the Degree

of

Master of Science in Mechanical Engineering

August 2009

Purdue University

West Lafayette, Indiana

To My Parents

ACKNOWLEDGMENTS

I owe my deepest gratitude to my thesis advisor, Prof. Steven Frankel for allowing me to join his research group, for his guidance, kindness, and most of all, his encouragement. My thanks and appreciation goes to my committee members, Prof. Jayathi Murthy and Prof. Fu Zhao. I am thankful to PEAT International, Northbrook, IL for financially supporting this work. I am very grateful to Jose Capote at PEAT for his timely feedback and encouragement. I am thankful to Dr. Abhilash Chandy for his help in understanding the research topic. I am greatly indebted to Dr. C. Praveen and Dr. Manoj T. Nair for introducing me to the field of CFD and encouraging me to pursue higher studies. I am thankful to Dinesh Shetty for his expertise, valuable guidance, readiness to help and making my work so much easier. I am grateful to Prof. Dong for his guidance and support. Finally, I would like to thank my parents for their love, continuous support and belief in what I do.

TABLE OF CONTENTS

LIST OF TABLES

LIST OF FIGURES

SYMBOLS

A	pre-exponential factor
m	mass
k	thermal conductivity
E_a	activation energy
R	universal gas constant
ρ	density
R_i	reaction rate for species i
J_i	diffusion flux for species i
h	specific enthalpy
C_p	specific heat
σ	Stefan Boltzman constant
ϵ	emissivity
μ	viscosity
T	temperature
t	time
r	radial distance
v	velocity
Y_i	species mass fraction
ΔH	heat of reaction
n_e	electron density
D	diffusion coefficient
Sc_t	turbulent Schmidt number
D_t	turbulent diffusivity
a	absorption coefficient

ABBREVIATIONS

CFD	Computational Fluid Dynamics
3-D	3 Dimensional
2-D	2 Dimensional
MSW	Municipal Solid Waste
PTDR	Plasma Thermal Destruction Recovery
WTE	Waste-To-Energy
MHD	MagnetoHydroDynamics
DAEM	Distributed Activation Energy Model
LTE	Local Thermodynamic Equilibrium
WTC	Well-Type Cathode
RTC	Rod-Type Cathode
NEC	Net Emission Coefficient
UDF	User-Defined-Function
UDS	User-Derined-Scalar
GTC	Gasification Technologies Council
EPA	Environmental Protection Agency
DRE	Destruction and Removal Efficiencies
TCLP	Toxicity Characteristic Leaching Procedure
SCADA	Supervisory Control and Date Acquisition
WSGGM	Weighted-Sum-of-Gray-Gases Model

ABSTRACT

Mashayak, Sikandar Y. M.S.M.E. , Purdue University, August 2009. CFD Modeling of Plasma Thermal Reactor for Waste Treatment. Major Professor: Dr. Steven Frankel.

Recently, thermal plasma process has been proved to be a viable technology for recovering energy and useful products from waste. The purpose of this work is to extend computational fluid dynamics (CFD) modeling to analyze and optimize design of industrial scale thermal plasma reactor for medical waste treatment. Overall technical review of plasma thermal waste treatment technology is provided. Plasma treatment of solid waste involves complex chemical and physical phenomena, such as pyrolysis, char gasication, gas phase reactions, solid-gas multiphase flow, turbulence, radiation heat transfer etc. The comprehensive modeling of these phenomena is an unreachable target.So, key approximations, based on experimental observations, are made in developing CFD model.

The thermal plasma reactor numerical model is implemented in the framework of commercial CFD code, FLUENT 6.3. Steady state incompressible Navier-Stokes equations are solved for basic fluid flow and physical sub-models used are: standard 2-eqn k-ϵ turbulence model, species transport with eddy dissipation kinetic model for gas phase reactions, P-1 model for radiation heat transfer and functional group approach with Arrhenius formulation for solid waste gasification. For non-transferred plasma jet, analytical model developed by [1] is employed. FLUENT model is developed for transferred plasma arc through user-defined functions (UDF), but it is avoided in reactor simulations for simplification. Numerical model is validated against experimental observations and then used in performance evaluation of different ge-

ometries of thermal plasma reactor. It is demonstrated that CFD model can be used for design analysis and optimization of thermal plasma reactor for waste treatment.

1. INTRODUCTION

Thermal plasma technology has been in use for a long time. It is well established in various processes, such as metallurgical processing, material synthesis etc. [2]. Only in recent years, it has been employed in treatment of organic waste. Thermal plasma is a promising technology for recovery of resources from non-conventioal sources like Municipal Solid Waste (MSW) and biomass residues [3]. It has various advantages over conventional waste incineration technology. It employs plasma torches to generate extremely high temperatures and transforms waste into synthesis gas, by pyrolysis and gasification chemical processes. Plasma pyrolysis converts organic part of waste into synthesis gas (CO and H_2), which can be used in gas turbines for power generation, and non-organic part of waste is transformed into non-leachable residue, useful in construction industry [3]. Plasma pyrolysis is neutral with respect to CO_2 emission, whereas conventional waste incineration of organic waste may utilize the energy content of waste but is associated with the generation of SO_2, NO_x and other hazardous emissions [4].

Despite important advantages, thermal plasma waste management technology is still under development and faces various technical and economical challenges [3]. Many social issues are associated with the use of materials produced by plasma treatment of wastes and are still an impediment to the broad use of waste materials in new products, affecting not only plasma technology but also other waste treatment processes. Although, it is clear that the avoidance of landfill charges, added value of the reuse of the vitrified product and energy production from synthesis gas, together improve the commercial viability of the process, significant developments are still required to make a large scale thermal plasma waste treatment facility economically viable.

Thermal plasma reactors are at the core of plasma waste treatment technology. Design optimization of reactor can play significant role in improving effectiveness and efficiency of converting waste into useful products. Computational Fluid Dynamics (CFD) has recently proved to be an effective means of analysis and optimization of energy-conversion processes [5]. Yang et al. [6] present applications of CFD tool in diagnosing waste incineration systems and evaluating changes in operating conditions. Ravelli et al. [5] have performed detail study on CFD modeling of bubbling fluidized bed combustion in waste-to-energy plants and demonstrated that a 3-D CFD-based model can successfully predict the behavior of fluidized bed combustion system. In similar study, Ryu et al. [7] demonstrate that CFD simulations can provide crucial information on the nature of chemical and flow characteristics and the subsequent gas flow pattern in the reaction chamber of a large municipal solid waste incinerator. Various other studies [8–11]have demonstrated that CFD can be effectively used in design evaluation and optimization of waste-to-energy process.

In this work, CFD model has been developed to simulate chemical processes, such as pyrolysis and gasification, and flow characteristics of industrial scale thermal plasma reactor for solid medical waste treatment. Plasma pyrolysis of solid waste involve various complex chemical and physical phenomena, such as pyrolysis, char gasification, gas phase reactions, solid-gas multiphase flow, turbulence, radiation heat transfer etc. Numerical modeling of individual phenomena is itself a challenging task. Hence, comprehensive numerical simulation of all these phenomena inside thermal plasma reactor is an unreachable target. As a result, key approximations, based on experimental observations, have been made in developing numerical model. This model is validated against experimental data and later used in evaluating different geometry configurations of reactor, based on product gas evolution and mixing.

In this report, first plasma technology is explained in general. Various configurations of plasma torches and their applications are described. Review on computational modeling of thermal plasma torch is provided. Then the plasma pyrolysis phenomena is explained in detail. Different reaction mechanisms and kinetics given

in the literature are presented. In the following chapter, working of industrial scale thermal plasma reactor, considered in this work, is explained. Various challenges and ways of overcoming it, in numerical modeling of solid waste pyrolysis are presented in the next review chapter. Then, the detail description of numerical model is provided. Geometry and grid of the different reactor configurations are explained. Various physical sub-models, discretization method and solution algorithm employed are described. Input data and boundary conditions used for simulations are given. Finally results of numerical simulations are discussed.

2. PLASMA TECHNOLOGY

2.1 Background

Plasma is often considered as the fourth state of matter. Gaseous plasmas consist of a mixture of electrons, ions, and neutral particles resulting from electrical discharge. The sun and the lightning are common examples of plasmas. In an electrical discharge the high-mobility electrons pick up energy from the applied electric field and transfer part of this energy to the heavy particles through collisions [12]. Depending on the amount of this energy transfer two types of plasmas are defined: *thermal* and *nonthermal* plasmas. Thermal plasmas approach local thermal equilibrium (LTE) because of high electron densities ($10^{21} - 10^{26}$ m^{-3}), resulting in high energy transfer to heavy particles. Whereas non-thermal plasmas have lower degree of ionization and lower energy densities, resulting in a large difference between the temperatures of the electrons and the heavier particles. They are often referred as "cold" plasmas [12]. The state parameters for each type of plasma are listed in Table 2.1.

There are numerous advantages of thermal plasmas: high temperature, high intensity, non-ionising radiation and high energy density. Thermal plasmas can reach temperatures of 20,000 K or more, whereas an upper temperature limit of 2000 K can be achieved by burning fossil fuels [3]. Because of these advantages thermal plasmas are employed in many industrial applications.

2.2 Applications

There has been a substantial growth in industrial applications of plasmas. In the beginning plasma technology applications were mainly in space related activities. Plasma gases were used to simulate high temperature conditions similar to

Table 2.1
Classification of plasmas [2].

Plasma	State	Example
High temperature plasma	T_e=T_i=T_h,T_p=10^6-10^8K, $n_e \geq 10^{20}m^{-3}$	Laser fusion plasma
Thermal plasma	$T_e \approx T_i \approx T_h$,$T_p$=$2\times10^3$-$3\times10^4$K, $n_e \geq 10^{20}m^{-3}$	Arc plasma;atmospheric RF discharge
Non-thermal plasma	$T_e \gg T_h \approx 3\times10^2$-$4\times10^2$K, $n_e \approx 10^{10}m^{-3}$	Corona discharge

Note: T_e = electron temperature;T_i = ion temperature;T_h = neutral temperature; T_p = plasma temperature; n_e = electron density

those when missiles re-enter the atmophere.Today thermal plasma technology covers a wide spectrum of applications as (1) thermal plasma coating techniques, like plasma spraying and plasma chemical vapor deposition (TPVD), (2) thermal plasma synthesis of fine powders, (3) thermal plasma densification of powders, (4) thermal plasma metallurgy, (5) thermal plasma extractive metallurgy [13]. The detail description of plasma technology application in waste destruction process is presented in the next chapter.

2.3 Plasma Generators

Plasma is generated by passing an electric current through a gas. Most gases are insulators at room temperature and hence, charge carriers must be generated to make the gas electrically conducting. The process of generating charge carriers in the gas is known as electrical breakdown. There are numerous ways in which electrical breakdown can be achieved. Most common way of generating plasma is by applying electric field between two electrodes, which causes breakdown of originally

nonconducting gas and the passage of an electrical current through the ionized gas leading to gaseous discharges. Other means of producing plasma include shock waves, laser or high-energy particle beams, heated gases in a high-temperature furnace [12].

The workhorse of plasma-assisted waste destruction is the plasma torch. Carbon electrodes were first employed for plasma-arc in 1960s as a source of intense heat [14]. There are many ways to generate thermal plasmas: DC electric discharges at electrical currents up to 10^5 A , alternating current (AC), or transient arcs (lamps,circuit-brakers or pulsed arcs), RF and microwave discharges at near-atmospheric pressure and laser-induced plasmas [3].

Plasma production methods in treat hazardous waste treatment include : DC plasma torches and inductively coupled plasma devices (RF) [3]. Plasma gases are extracted as a jet through an opening in the electrode and out of the confines of the cathode-anode space. The unstable arc column is stabilized by forced gas flow along the current path or by interaction with a guiding wall or by external magnetic fields [14].

2.3.1 DC Plasma Torches

Plasma arc generators in material processing mostly employ DC rather than AC, because there is less flicker generation and noise, a more stable operation, better control, a minimum of two electrodes, lower electrode consumption, slightly lower refractory wear and lower power consumption [3]. DC plasma torches are characterized by a high energy density and high temperature region between two electrodes. The plasma can extend beyond one of the electrodes in the form of jet if gas flow rate is sufficiently high. DC arc torches are typically available at power levels up to 1.5 MW and the temperature in the core of plasma can be greater than 30,000 K [2]. Under oxidative conditions electrodes may gradually abate and contaminate the products. The processes, where product contamination due to electrode erosion is unacceptable, usually employ inert (nonoxidizing) plasma-forming gases like Ar, Ar/H_2,Ar/He,Ar/N_2, etc. However, in waste treatment process product contamina-

tion is not of concern and hence, air, which is cheaper and simpler alternative to Ar, can be used as plasma gas. The average lifetime of electrodes ranges from 200 to 500 hours of operation [2]. Due to relatively short electrode lifetimes DC arc plasma melting and waste treatment systems are generally implemented as batch processes [15].

DC arc plasma generators can be divided into two groups: non-transferred arc torch and transferred arc torch. The brief description of both kinds is given below:

2.3.1.1. Non-transferred Arc Torches

DC non-transferred arc torches are commonly used devices in material processing using plasma technology. An arc is struck between a concentric cathode and anode. Plasma gas is then passed through electric arc producing a hot jet, coming out of nozzle. The electrode material can erode gradually and hence, to prevent that electrodes are made larger and generally water cooled. Such type of torch can contaminate the product and have very low energy efficiencies (as low as 50%) [3].

Non-transferred arc DC torches are mainly used in two configurations : with hot electrodes and with cold electrodes. DC torches with hot electrodes typically operate at power levels below 100 kW and are made up of thoriated tungsten cathode and an annular copper anode. Oxidizing gases can not be used, as they may oxidize the tungsten electrode. The plasma temperatures are between 6,000 and 15,000 K, with energy densities of around 145 MJ/m^3 and gas flow rate is generally below 6 m^3/h. Whereas, DC torches with cold electrodes are made up of cold, copper electrodes of very high thermal conductivity and can be used with oxidizing plasma gases. The plasma is generated with a strong vortex motion between two coaxial, tubular electrodes separated by a small gap. They can reach power levels from 100 kW to 6 MW with temperatures up to 8,000K and gas flow rates as high as 300 m^3/h in a 1 MW torch [3].

2.3.1.2. Transferred Arc Torches

In transferred arc torches, only one of the plasma forming electrodes is contained within any single torch body and other electrode work-piece is located outside

the torch. The separation between torch electrode and work-piece electrode can range from a few centimeters to almost 1 m. Cathodes are generally made up of either a water-cooled or a refractory material that is consumed slowly, e.g. graphite, tungsten or molybdenum. Anodes are usually flat ended cylinders made up of metals with high thermal conductivities, such as copper or silver. Torch can be anodic or cathodic depending on the application and operating conditions. Anode torches are particularly beneficial when no contamination from the electrode can be tolerated, e.g. melting of titanium where tungsten contamination is unacceptable [3].

In most waste destruction applications graphite is used for electrode material, because carbon contamination from electrode wear is not a problem. Being refractory material, it is a simpler and cheaper alternative to water-cooled torches. Also it can be used with diatomic gases and therefore nitrogen/air can be used as a cheaper alternative to argon gas.

DC transferred arc torches are more efficient than non-transferred arc torches, because the plasma arc is located outside the water-cooled body of the torch which minimizes the radiant heat transfer losses to the cold torch body resulting in high thermal fluxes. Another advantage of transferred arc is that they can be used in a couple twin-torch mode, where anode and cathode are both torches producing a coupled plasma. This arrangement does not require the work-piece and is ideal for the melting of non-conducting materials and in-flight vaporisation of powders [3].

2.3.2 RF Plasma Torches

RF plasma torches transfer electromagnetic energy from the RF power source to the plasma gas by inductive or capacitive coupling. Hence plasma gas does not come in direct contact with electrodes, which avoids the contamination of the plasma by metallic vapors. They are commonly available at power levels of 100 kW and the temperature at the central channel can reach up to 6000 K [2]. The industrial applications of RF plasma torches include spectrochemical analysis, synthesis of high-purity silicon or titanium dioxide pigments, and ultra-fine and ultra-pure power synthesis [3].

RF plasma torches are being increasingly considered for material processing. They are compact and deliver high input energy per unit volume. As electrodes of RF torches are not exposed directly to the severe conditions, they have a very long lifetime. Though DC plasma torches generate the stable arcs, they require expensive electronics and controls and the plasma plume is very narrow. Whereas RF plasma torches generate a very diffuse plume and the design of external electrodes favors the injection of feedstock directly into or through the plasma region. But use of oscillator electronics severely limits the efficiencies of RF plasma systems [2].

Table 2.3.2 presents the comparison of the main features of different plasma processes for waste treatment.

Table 2.2
Comparison of different plasma processes for waste treatment [2].

Item	DC arc plasma	RF plasma
Temperature	5,000-10,000K	3,000-8,000K
Electrode erosion	Yes, (1000-3000 h lifetime in inert gas, 200-500 h lifetime in oxidative gas)	No
Cooling	Required	Required
Plasma ignition	Easy	Difficult
Plasma volume	Small	Medium
Gas velocity	High	High
Solid feeding position	Downstream of plasma	Upstream of plasma
Influence of solid feeding on plasma stability	No	Yes
Efficiency of power supply	60-90%	40-70%

2.4 Review of Thermal Plasma Model

Substantial growth in industrial applications of plasma torches make it imperative to understand flow structures, heat, mass and momentum transfer in plasma gases, so that necessary improvements in design of plasma torches can be made. The modeling of thermal plasma processes involve complex physical and chemical phenomena like fluid dynamics, turbulence, interactions between electric discharge and gas flow, mixing with the surrounding atmosphere, injection of cold gases into the plasma stream, fluid-particles interactions, and chemical reactions [16]. Experimental work on the plasma process is limited because of its complexity and hence, numerical simulations are important to obtain detail informations about plasma processes [17]. Numerical simulations of such complex phenomena is made feasible with recent advancements in computational hardware and the 2D modeling is progressively being replaced by 3D models. However, comparison and validation of 3D models of plasma process remain difficult [18]. Despite the progress in simulation tools, lot of work remains to be done in describing plasma-particle interaction in the context of DC plasma spraying, as experimental in-flight particle data are often not reproduced adequately [19]. Nevertheless, two-dimensional axisymmetric modeling of plasma torches are still widely performed to design and optimize the plasma torches for various applications.

Plasma spraying is one popular application of plasma torches. It involves treatment of powdery material in plasma. Information about characteristics of plasma gases is critical to understand particle trajectory and heat transfer. Significant work is done in numerical analysis of plasma torches with plasma spraying as research background. Eichert et al. [20] present numerical model to predict the plasma jet behavior to understand cooling of the jet and mixing, to guide actual experimental works by defining ranges of values for spraying parameters to be optimized and to help in the definition and design of spray torch nozzles. The flow of an ArH_2 gas mixture through a DC plasma torch is simulated using CFD PHOENICS code. Equations of mass,

momentum and energy along with k-ϵ two-equations turbulent model are discretized by control-volume method and solved by the SIMPLEST algorithm. Assumptions of local thermal equilibrium (LTE) and chemical equilibrium are made. Also radiation phenomena, gravity effects and electro-magnetic forces are neglected. The local arc phenomena is not modeled. Only the thermal effects of the arc on the gas flow are considered through energy source term, which is set equal to torch power. The ArH_2 mixture properties are modeled as polynomial of temperature at constant pressure.This model allows to obtain the temperature and velocity profiles at the torch exit as a result of basic phenomena occurring inside the torch.

Han et al. [21] present modeling of the subsonic-supersonic flow and heat transfer in a DC plasma torch used for low-pressure (soft vacuum) plasma spraying. 2D axisymmetric approach is used with assumptions of steady, laminar flow and plasma is assumed to be in local thermal equilibrium. Full Navier-Stokes equations, along with electromagnetic governing equations and source terms are solved using the all-speed SIMPLE algorithm, which is an extended form of the standard SIMPLE algorithm in order to be applicable to the case of compressible flow. FAST-2D CFD program is used with some modifications, so that variable plasma properties and the all-speed SIMPLE algorithm can be employed. Pure Ar is used as plasma forming gas, with thermophysical properties as a function of temperature and pressure. Empirical relation is used to model the volumetric radiation power of argon plasma. The results present the distributions of the temperature, velocity, static pressure, and Mach number within torch. It is concluded that gas viscosity and the Lorentz force have very little effect on the results.

Nozzle configuration may have significant effects on characteristics of plasma. Work of Yuan et al. [22] is another example of numerical study of DC plasma torch, with plasma spraying as the research background. They investigate effects of nozzle configuration on the characteristics of flow inside the DC plasma torches by numerical simulation. The assumptions of axisymmetric, LTE and steady-state plasma are made. Pure Ar, with temperature and pressure dependent properties, is used as

plasma gas. Radiation loss is modeled using empirical approach. Governing equations of flow and electromagnetic effects are solved using PHOENICS 3.3 CFD code based on finite volume method. The results are validated with experimental data and it is observed that torches with different anode nozzle configurations produce different plasma flows, as expected.

Numerical studies of plasma arc used for waste treatment have also been performed. Paik et al. [17] numerically studied flow and heat transfer in an electric arc furnace for waste minimization. Soil is used as a substitute to the waste and liquid-solid phase of the molten solid, along with the plasma phase of the arc are simulated simultaneously. One of the assumptions is that interface between the plasma arc and the molten pool is fixed as a flat surface, for simplicity. Also, material volatilization effects at the plasma-molten pool interface are not included. Using this model, parametric study is done on different arc lengths and arc currents with varying input powers.

In another study, involving a waste melting process, Hur et al. [23] perform numerical analysis and experiments on transferred plasma torches, for finding appropriate operating conditions and electrode configuration. Six different electrode arrangements, consisting of a conical rod cathode and a nozzle in the torch, and a distant anode material, are studied. The heat transfer rate, from arc column to melted material, is predicted. Finally, optimized configuration of transferred plasma torches are presented for waste melting process.

Some industrial DC transferred plasma torches are equipped with a well-type cathode (WTC). Chau et al. [24] performed numerical simulation of 1.2 MW DC transferred well-type plasma torch. Coupled flow and magneto-hydrodynamic (MHD) equations are solved using a finite volume discretization method. Mixture of air and N_2 plasma forming gas is approximated by assuming pure N_2 gas. Flow is modeled as axisymmetric, steady state, LTE and the turbulent effects are neglected. The temperature and velocity distributions obtained using this model confirm difference

between rod-type cathode (RTC) and the cold cathode in WTC. The results are validated against the experimental data.

Freton et al. [25] also perform a numerical 3-D modeling of hollow cathode torch, for representing the arc movement and studying the convection effects within the cathode. Effects of vortex and magnetic forces are observed. The results obtained help to understand the hydrodynamic flow in the hollow cathode geometry and explain the action of magnetic coil on the electric arc.

Seo et al. [26] numerically analyze the influence of DC arc jets on the flow fields in a hybrid plasma torch, by an integrated direct current-radio frequency (DC-RF) plasma model, based on magneto-hydrodynamic (MHD) formulations. The continuity, momentum and energy equations, including effects of MHD, for the DC arc jet and RF plasma are integrated and solved in entire region of a DC-RF hybrid plasma torch. Assumptions of laminar axisymmetric flow with local thermal equilibrium (LTE) are made and Ar is chosen as a plasma gas, with properties evaluated at atmospheric pressure and 5000 K. The effects of DC arc gas flow rate, swirl in sheath gas flow and DC input current on the flow fields of the DC-RF hybrid plasma are studied.

Radiation plays very critical role in the energy transport in thermal plasmas. Exact formulation of radiation in plasma is very complicated procedure. One has to account for the emission and absorption over whole spectral range. Whereas, spectrum is composed of a continuous and a line spectrum, which is determined by energy levels of the atoms and molecules of the gas [27]. Menart et al. [28] present a computer simulation of a thermal plasma, that utilizes a detailed line-by-line radiative analysis coupled to a flow and temperature fields. Coupled governing equations are solved using finite-volume method and radiative transport is modeled with S-N discrete ordinate method. Radiative transport properties are calculated from atomic data. Noticeable differences are observed, when results are compared with an uncoupled analysis using net emission coefficients. However, the computational times are found to be quite large.There are different alternative approaches to account for ra-

diation in numerical modeling of plasmas, like using net emission coefficients (NEC), P-1 approximation, the partial characteristics method.

Karetta and Lindmayer [27] present simulation of the gasdynamic and electromagnetic processes in low voltage switching arcs, with very simplified approach to model radiation. A three-dimensional (3D) simulation model is described, which integrates the effects of electromagnetic processes on the gasdynamic of the electric arc. The coupled governing equations are solved by a commercial CFD code CFDS-FLOW3D, using self-written routines. One of the assumptions made is simplified radiative cooling approach. Because of complications in modeling exact energy transport by radiation in plasma, only the heat loss by radiation using Stefan's law is modeled. The absorption coefficient of the plasma gas is assumed to be independent of temperature and linearly dependent on pressure. The motion of arc in a simple arc chamber is simulated using this model.

Use of net emission coefficients (NEC) is an approximate, but computationally convenient method to account for radiation in plasmas [29]. To use this approach, one has to know the value of net emission coefficient for plasma-forming gas, which depends on temperature and pressure. As Ar is used in many applications for plasma gas, literature is available on NEC of Ar gas [30]- [31]. Naghizadeh-Kashani et al. [32] present net emission coefficients of air thermal plasma, which is used in waste treatment applications.

Kotalik [33] presents modeling of an argon plasma flow using NEC model to calculate radiation. MHD governing equations are nondimensionalized and solved numerically, using backward Euler scheme in time, and continuous piecewise linear finite elements on triangular meshes in space. The temperature dependence of net emission coefficient is taken into account. It is found that radiative losses increase with increasing currents and flow rates. Dependence of results on the choice of the optical thickness of the plasma column, which affects the value of NEC, is also observed. Results are validated against experimental data.

However, NEC modeling approach only gives an approximation of the net radiation leaving the hot part of the plasma and fails to represent the strong self-absorption of an important part of the spectrum at the cold boundary of the arc [34]. P-1 radiation model makes it possible to account for both, emission and self-absorption. Eby et al. [34] model the radiative transfer in SF_6 circuit-breaker arcs, with the P-1 approximation. P-1 approximation equations, along with spectral aspects of radiation, are described. Finite Volume methods are used to solve P-1 equations and gas flow governing equations. The results are compared with data obtained using net emission coefficients and partial characteristics approach. The results obtained show that good agreement is attained with both methods. According to authors P-1 approximation is a viable alternative to model radiation in a transient arc flow, from an efficiency and an accuracy point of view.

Sun et al. [35] present the 3D numerical analysis, with P-1 radiation model, in low voltage switching arc. Coupled equations of electric field, magnetic field, flow field and thermal field are solved using commercial CFD code FLUENT. The effects of both, emission and self-absorption, are taken into account. The radiation energy is calculated using P-1 model, with the spectrum divided into six bands. Approximation of local thermal equilibrium is made. And the air arc medium is assumed as gray body, which has absorption and scattering coefficients independent of wavelength. The distributions of temperature, radiation energy flux and flow field in low voltage switching arc are investigated with this model. Results are compared with that of net emission coefficient (NEC) method and obvious temperature differences are discussed. Values of arc column voltage by P-1 model are lower than the one by NEC method, but they are close to the experimental results.

It can be observed from the works mentioned in this section that most of the plasma arc numerical simulations are performed in commercial CFD code FLUENT. This approach is based on mainly implementing the additional governing equations of electrical potential and potential vectors along with heat sources through an external user-defined function (UDF). Bernardi et al. [36] present different techniques for the

FLUENT-based treatment of the electromagnetic field in inductively coupled plasma torches. Using the framework of FLUENT, they perform computations for LTE, optically thin argon plasmas at atmospheric pressure. By default FLUENT solves all the fluid dynamic variables everywhere in the domain, including outside region of the torch, when a far field approach is used for the treatment of the electromagnetics of the system, which may result in numerical instabilities and convergence issues. Authors, here, present a new technique for the simulation using FLUENT, allowing solutions of vector potential equations in a domain restricted to the torch region. It is shown that, their new technique is up to 60 % faster per iteration, when compared to user-defined scalars (UDS) approach.

In this work, air is used for plasma gas and its properties are calculated as a functions of temperature, at atmospheric pressure. Analytical model is used to calculate velocity and temperature at the exit of non-transferred plasma torch. Whereas, FLUENT model is developed to simulate transferred plasma arc. Appendices A, B and C provide the description of air plasma physical and thermal properties, non-transferred arc analytical model and FLUENT model for transferred arc, respectively.

3. PLASMA PYROLYSIS

3.1 Pyrolysis

Pyrolysis has been in use since the dawn of civilization. The ancient Egyptians practiced wood pyrolysis for tars and pyroligneous acid to be used in their embalming industry [37]. Since then wood pyrolysis, also called as wood distillation, has been in practice as a fuel supply process, until the advent of petrochemical industry in the 20th century. However, exponential growth of energy demand combined, with depletion of fossil fuels and increasing environmental consciousness, have made it necessary to use renewable sources of energy. Pyrolysis is one of the most efficient ways of obtaining energy from renewable energy sources, such as biomass, and solid waste .

Pyrolysis is the thermal processing of organic substances, like waste and biomass, which are thermally unstable, in the *complete absence of oxygen*, to split them into gaseous, liquid, and solid fractions, through a combination of thermal cracking and condensation reactions [38].

The major products formed during pyrolysis process are as following [38]:

1. A gas stream containing primarily hydrogen (H_2), methane (CH_4), carbon monoxide (CO), carbon dioxide (CO_2), and various other gases, depending on the organic characteristics of the material.

2. A liquid fraction, containing tar or oil stream consisting of acetic acid, acetone, methanol, and complex oxygenated hydrocarbons.

3. A char, consisting of almost pure carbon plus any inert material, originally present.

When a biomass particle is heated in inert atmosphere, the overall pyrolysis process takes place in two stages, primary and secondary stages. First, heat is transferred to the particle by radiation and convection. With the increase in temperature, moisture inside the particle is removed. Then the pre-pyrolysis and main pyrolysis reactions take place. These reactions are highly endothermic, resulting in temperature gradients. The formed volatiles and gaseous products then flow through the pores of particle and participate in the heat transfer process. The rate of pyrolysis depends on the the local temperature [4].

The product composition of pyrolysis process largely depends on the temperature, at which the process is carried out. Gas composition as a function of temperature is given in Table 3.1 .

Table 3.1
Gas composition for pyrolysis as a function of temperature [38].

Gas	Percent by volume			
	900^{o}F	1200^{o}F	1500^{o}F	1700^{o}F
H_2	5.56	16.58	28.55	32.48
CH_4	12.43	15.91	13.73	10.45
CO	33.50	30.49	34.12	35.25
CO_2	44.77	31.78	20.59	18.31
C_2H_4	0.45	2.18	2.24	2.43
C_2H_6	3.03	3.06	0.77	1.07

The pyrolysis process can be classified into 3 subclasses: conventional pyrolysis, fast pyrolysis, and flash pyrolysis [39]. The range of the operating parameters for these processes are given in Table 3.2 .

Conventional pyrolysis is characterized by a slow heating rate. Solid, liquid and gaseous pyrolysis products are significant in this condition. In the prepyrolysis stage, some internal rearrangement, such as water elimination, bond breakage, appearance

Table 3.2
Range of the main operating parameters for pyrolysis processes [39].

	Conventional Pyrolysis	Fast Pyrolysis	Flash Pyrolysis
Pyrolysis Temperature (K)	550-950	850-1250	1050-1300
Heating Rate (K/s)	0.1-1	10-200	>1000
Particle Size (mm)	5-50	<1	<0.2
Solid Residence Time (s)	450-550	0.5-10	<0.5

of free radicals and formation of carbonyl, carboxyl, and hydroperoxide groups, takes place. It is followed by main pyrolysis process in which decomposition of solid takes place. It is pyrolysis process and proceeds very fast. Slow decomposition of char takes place in third stage and carbon-rich residual solid is formed [39].

Fast pyrolysis is recommended when liquid and/or gaseous products are required. Fast heating rates are achieved by high temperatures, very short contact times, and very fine particles. Higher efficiency is achieved by the so-called flash pyrolysis, where finely divided feedstock is quickly heated to between 1050 and 1300 K for less than a second.

In general, when waste is treated by pyrolysis process, the pyrolysis is followed by gasification of produced volatiles and char. The brief description of gasification process is given in the following section.

3.2 Gasification

The gasification process was discovered in the nineteenth century. Recently it has been applied to the processing of solid waste. The GTC defines the gasification as [40],

- A process technology that is designed and operated for the the purpose of producing synthesis gas through the chemical conversion of carbonaceous materials.
- A process that converts carbonaceous materials through a process involving partial oxidation of feedstocks in a reducing atmosphere in the presence of steam at temperatures sufficient to convert the feedstock to synthesis gas; to convert inorganic matter in the feedstock to a glassy solid material, known as vitreous frit or slag; and to convert halogens into the corresponding acid halides.

In the gasification process, after chemical bonds are broken by thermal energy and not by oxidation (i.e. by pyrolysis), partial combustion of volatiles and char takes place with less than stoichiometric oxidizer. Due to insufficient oxygen, oxidation is limited and thermodynamic and chemical equilibria of the system shift to reduced rather than an oxidized state. Although pyrolysis reactions are endothermic, gasification of volatiles and char are mostly exothermic reactions. Product of gasification is a combustible fuel gas rich in carbon monoxide, hydrogen, and some saturated hydrocarbons, principally methane [38, 40].

3.3 Advantages of Gasification

Conventional incineration of waste is merely burning it in the presence of excess oxygen, to maximize the conversion of the hydrocarbon-based wastes to carbon dioxide and water.

Incinerators have significant pollution problems. SO_x and NO_x are formed from sulfur and nitrogen in the feedstock, while halogens in the feedstocks get converted into acid gases such as HCl and HF. Due to requirement of excess air in the incineration chamber, the temperature of incineration process is limited. Incomplete combustion and low temperatures may produce extremely toxic products like furans and dioxins [14].

Whereas, gasification process is characterized by high temperatures and very little oxidation. This results in production of more syngas and not CO_2. Due to

reducing environment in the gasification chamber formation of SO_x and NO_x is prevented. Instead, sulfur and nitrogen in the feedstock are converted to H_2S, ammonia and nitrogen. Halogens in the feedstock are converted to inorganic acid halides, which can be removed from the syngas in downstream cleanup operations [40].

Key differences in gasification and conventional incineration technologies are presented in Table 3.3.

3.4 Thermal Plasma Pyrolysis

Thermal plasma pyrolysis is the technology, which integrates the thermo-chemical properties of plasma with the pyrolysis process. The presence of charged and excited species, together with the high energy radiation, makes the plasma environment highly reactive and it can catalyse homogeneous and heterogeneous reactions [14].

Thermal plasma pyrolysis has several advantages over standard gasification process. In standard gasification technology temperature is in the range 600-1000 K. Mostly they rely on the process itself to sustain the reaction and do not use any external heat source. Although this process produces a fuel gas similar to the gas produced by plasma process, it is much dirtier and contains char, tars and soot, because lower temperatures can not break down all the materials. As a consequence, many materials must be sorted out of the waste stream before reaching the reactor and landfilled or processed in other ways. Also, the char produced is upto 15% of the weight of the incoming material and must be landfilled. In contrast, plasma gasification uses an external heat source to gasify the waste and hence results in very little combustion. Almost all of the carbon is converted into fuel gas. In fact, plasma gasification is the closest technology available to pure gasification. Very high temperatures promote complete break down of all the tars, char and dioxins. Hence the fuel gas is much cleaner and very little ash is generated [41].

Table 3.3
Key Differences between Gasification and Incineration [40].

Subsystem	Incineration	Gasification
Combustion vs. Gasification	Designed to maximize the conversion of feedstock to CO_2 and H_2O	Designed to maximize the conversion of feedstock to CO and H_2
	Large quantities of excess air	Limited quantities of oxygen
	Highly oxidizing environment	Reducing Environment
	Operated at temperatures below the ash melting point. Mineral matter converted to bottom ash and fly ash.	Operated at temperatures above the ash melting point. Mineral matter converted to glassy slag and fine particulate matter (char).
Gas Cleanup	Flue gas cleanup at atmospheric pressure	Syngas cleanup at high pressure.
	Treated flue gas discharged to atmosphere	Treated syngas used for chemical production and/or power production (with subsequent flue gas discharge).
	Fuel sulfur converted to SO_x and discharged with flue gas.	Recovery of reduced sulfur species in the form of a high purity elemental sulfur or sulfuric acid byproduct.
Residue and Ash/Slag Handling	Bottom ash and fly ash collected, treated, and disposed as hazardous wastes.	Slag is non-leachable, non-hazardous and suitable for use in construction materials. Fine particulate matter recycled to gasifier or processed for metals reclamation.

In addition, thermal plasma process offers a range of other advantages [3]:

1. Compact reactor geometry with high throughput.
2. Specific gas and solid material compositions can be obtained due to high quench rates ($> 10^6$ K/s).
3. Allows low gas flow rates (except for non-transferred plasma devices) compared to the combustion of fossil fuels, thereby reducing the requirements for off-gas treatment.

When carbonaceous particles are injected into a plasma, approximately four stages take place in the thermal plasma pyrolysis [2]:

1. A very fast heating of the particles as a result of their heat exchange with the plasma jet.
2. An explosive liberation of volatile matter from the particles.
3. A very quick gasification of the homogeneous phase and rapid heat and mass exchange.
4. Further gasification of char particles with various gaseous components.

When injected into the plasma, particles are heated rapidly, resulting in release of volatile matter, hydrogen, light hydrocarbons (such as methane and acetylene) and a solid residue with varied properties, depending on the feed characteristics and operating conditions. To achieve certain technical purposes, such as monomer recovery stage 3 could be replaced by quench process. Also, additional water or steam can be used in stage 4 to increase syngas (H_2 and CO) production.

Plasma pyrolysis technology have previously been applied in the coal gasification process. Kalinenko et al. [42] have performed number of experiments on the plasma-vapor gasification of brown coals, using an experimental plant with electric-arc reactor. They observed 90.5-95.0 % degree of gasification and 84.7-85.7 % concentration of the syngas. Georgiev et al. [43] studied steam plasma gasification of solid fuel.

Authors investigated coal gasification in a water steam plasma. Coals with different ash contents were gasified and it was shown that there is a difference in plasma gasification for low and high ash coals. Djebabra et al. [44] discussed influence of several parameters on the H_2 and CO yields from gasification of a coal by microwave plasma water vapor.

Extremely high temperatures and capability of significantly decreasing the waste volume to a non-leachable residue, have increased development of plasma applications in waste management. Although, initially focus was on the destruction of hazardous wastes rather than energy recovery, in recent years, the interest in energy and resource recovery from waste has grown significantly [4]. Nema et al. [14] present the thermal plasma pyrolysis of medical waste at the Facilitation Centre of Industrial Plasma Technologies, Institute for Plasma Research, Gandhinagar, India. Different stages in medical waste pyrolysis reactor, along with various subsystems involved are described. Medical waste is simulated using cotton and plastic $(2 : 1)$ and gas chromatography results of the plasma pyrolysis reveal that product gas is rich in hydrogen and carbon monoxide, with some lower hydrocarbons. Finally, the economic viability of plasma pyrolysis of medical waste with energy recovery option is calculated. The calculations show that if energy is recovered from the pyrolysed gases of medical waste, the destruction of approximately 600 kg waste per day for typically 50 kW system is enough to break even.

Gomez et al. [3] present a critical review of thermal plasma technology for treatment of wastes. Authors describe the current status of waste treatment using thermal plasma technology. It is concluded that thermal plasma is a promising alternative to conventional and industrially mature thermal processes for waste treatment. Tang et al. [45] present experimental results of plasma pyrolysis of polypropylene in a dc arc nitrogen plasma generator and show that plasma-assisted thermal decomposition of polypropylene may be a useful way for recovering energy and useful chemical from waste plastics. Moustakas et al. [46] designed a pilot plasma gasification system and demonstrated effectiveness of plasma treatment of hazardous waste. Mountouris et

al. [47] present a case study of plasma gasification of sewage sludge at the Athens' Central Wastewater Treatment Plant (Psittalia Island). An integrated process is proposed and optimized to demonstrate that plasma treatment of 250 ton/day sewage sludge with 68% moisture results in a net production of 2.85 MW electrical energy.

Process overview of thermal plasma treatment of solid waste is described in the following section.

3.5 Process Overview

Process diagram of a typical system for plasma gasification of solid waste is represented in Figure 3.1. Plasma gasification plant consists of many sub-systems like waste feed system, a primary reaction chamber (plasma furnace), a secondary reaction chamber, a solid residue remover, a gas cleaning and conditioning unit, a water cooling system, operation control and data acquisition and monitoring unit.

Waste Feed

The waste feed sub-system is used to treat each type of waste in order to meet the inlet requirements of the plant. A typical feed system consists of a shredder for solid waste size reduction before it enters the plasma furnace. If high moisture is present in the waste material then a drier is used [41].

Plasma Furnace

Primary reaction chamber is a plasma arc furnace with one or more plasma torches. Mostly air is used as plasma forming gas, because it is a cheaper alternative to Argon or other inert gases. It operates under controlled reducing conditions and runs at temperature above 1500K. In here, the main pyrolysis and gasification of waste material take place. Product gases are sent through outlet to cleaning unit, while solid slag is collected at the bottom. The electrical power supply depends on throughput, but is usually of the order of a few MW and is controlled independently [3].

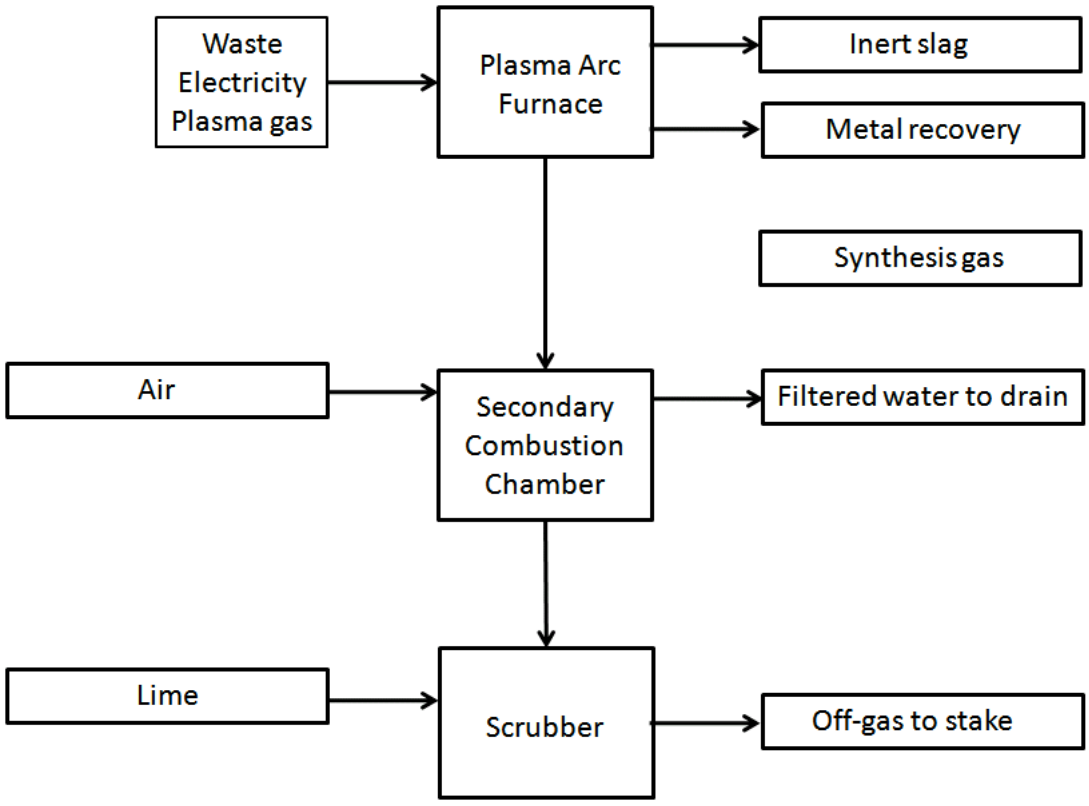

Figure 3.1. Process diagram for the plasma gasification of waste [3].

Secondary Reaction Chamber

The syngas from plasma furnace is then further processed in a secondary reaction chamber. Depending on the waste being processed, the syngas can be further conditioned to be used in several energy recovery options.

Gas Cleaning Unit

The resulting gas from secondary reaction chamber is then fed through a gas cleaning and conditioning system. Here, the gases are rapidly cooled to ensure that there is no potential for the generation of undesired compounds. The gas cleaning unit achieves the elimination of acid gases, particulate matter, heavy metals and moisture from the syngas.

Energy Recovery Unit

After cleaning, the syngas can be used as a fuel to produce steam for steam turbine and generate electricity. If energy recovery unit is not available, the syngas can be transformed to produce nitrogen, oxygen, carbon dioxide and water vapor.

For more details about working of commercial thermal plasma unit for waste destruction refer to chapter on plasma thermal reactor.

3.6 Reaction Mechanism And Kinetics

Thermal conversion of waste involves various chemical and physical processes, such as vaporization, devolatilization (pyrolysis), volatile secondary reactions, char oxidation, coupled with transport phenomena. Understanding evolution of different species in the waste thermal treatment is important in design process of thermal plasma reactors. The composition of product gas and rate of formation of each species depend on the operating conditions, like temperature, pressure, velocity, residence time etc. Hence, a mathematical model, which can relate different operating conditions to evolution of product species is required. Also, such a model is critical in developing numerical tool for analyzing thermal plasma reactor design.

The reaction mechanism of pyrolysis process is very complex and difficult to model. Nature and constituents of solid waste vary widely depending on the source and conditions. Hence, it makes more difficult to model standard reaction mechanism for gasification of solid waste. Due to rising interest in gasification of waste, various experimental and numerical studies have been published in the literature on gasification of biomass,wood, medical waste, polypropylene etc. Overview of different reaction mechanisms and reaction kinetics explained in these studies is presented in following sections.

3.6.1 Review of Reaction Mechanism

Babu [4] presents pyrolysis reaction mechanism for polymer molecules. The pyrolytic reactions are broadly classified into four groups: random main-chain scission, depolymerization, carbonization, and side-group reactions. In random-chain scission, breaking of the main chain takes place to produce smaller molecules of random sizes. Successive removal of monomer units from the chain is defined as depolymerization and it leads to the formation of free radicals and chain reactions. In carbonization and side-group reactions, cross-linking, straight chain polymer formation, cyclization, and aromatization by dehydrogenation occur. Both chain scission and depolymerization mechanisms involve initiation, propagation, chain transfer, and termination reactions.

As per standard Gibbs free energy for the reactions, energy requirement for C-C bond cleavage is less than hydrogen abstraction. Also, the chain scission of C-C bonds at the ends of molecules is more probable than at the center of the molecule. In plasma reactor, collisions between the polymer molecules and electrons and ions from the plasma initiate the β-scission process. This is followed by series of reactions which convert the polymer fragments into reactants and, subsequently, to final products through radical decomposition, radical isomerization, hydrogen tansfer, and/or radical addition. Chain of reactions is terminated when two radicals combine or disproportionate to form stable products. Relative sensitivity of secondary and primary reactions result in range of product compositions, depending on the temperature and residence times in the high-temperature plasma region.

3.6.2 Reactions

Tang et al. [45] studied kinetics, catalysis, and reaction engineering of plasma pyrolysis of polypropylene for converting waste plastics into gaseous fuel and useful chemicals. It is observed that hydrogen and acetylene are the main components of the gas produced in the plasma reactor. The possible reactions presented are as follows:

$$R_1CH_2CHCH_3CH_2CHCH_3R_2 \rightarrow R_1CH_2CHCH_3^{\bullet} +^{\bullet} CH_2CHCH_3R_2 \qquad (3.1)$$

$$^{\bullet}CH_2CHCH_3CH_2CHCH_3R_3 \rightarrow CH_3CH = CH_2 + ^{\bullet}CH_2CHCH_3R_3 \tag{3.2}$$

$$CH_3CH = CH_2 \rightarrow CH_4 + C_2H_2 \tag{3.3}$$

$$CH_3CH = CH_2 \rightarrow 3C + 3H_2 \tag{3.4}$$

$$CH_3CH = CH_2 \rightarrow C + 2H_2 + C_2H_2 \tag{3.5}$$

where,

R_1 is $(-CH_2CHCH_3-)_l$,R_2 is $(-CH_2CHCH_3-)m$, and R_3 is $(-CH_2CHCH_3-)_n$.

Reaction (3.1) is the initiating reaction, reaction (3.2) is the β-scission reaction. These two reactions are generally accepted in thermal degradation of polypropylene. Reactions (3.3)-(3.5) are some of the possible reactions for formation of hydrogen, acetylene, and methane.

In conventional gasification process, equilibrium state is not reached, because the temperature is sufficiently below 1000 K. Whereas, in higher temperatures of plasma gasification process, equilibrium is attained, given that residence time is sufficiently long. Huang et al. [48] describe the equilibrium composition of the typical medical waste under high temperature pyrolysis, using NASA CEA2 program. The calculations results indicate that product gas mainly contains CO and H_2, with other components such as CO_2, C_2H_4, C_2H_2,CH_4 etc. Mountouris et al. [41] present equilibrium model for solid waste plasma gasification.The equilibrium model development is based on the chemical reactions that describe better the gasification process. The solid waste material is described by its ultimate analysis ($C_xH_yO_z$) and the global gasification reaction is written as:

$$\begin{aligned} CH_xO_y + wH_2O + mO_2 + 3.76mN_2 =& n_1H_2 + n_2CO + n_3CO_2 + n_4H_2O + n_5CH_4 \\ &+ n_6N_2 + n_7C \end{aligned} \tag{3.6}$$

where w is the amount of water per kmol of waste material, m is the amount of oxygen per kmol of waste, n_1,n_2,n_3,n_4,n_5,n_6,n_7 are the coefficients of the gaseous products and soot.

The equilibrium is calculated using mass and energy balances, along with three independent reactions involving CH_4, CO, CO_2,H_2, H_2O and C (soot). The specific heat and enthalpy changes of the gas products are expressed as a function of the gasification temperature as will as equilibrium constants of the chemical reactions, which are:

$$CH_4 + H_2O = CO + 3H_2 \tag{3.7}$$

$$CO + H_2O = CO_2 + H_2 \tag{3.8}$$

$$C + H_2O = CO + H_2 \tag{3.9}$$

Nema et al. [14] simulated hospital waste with cotton and plastic (2:1) to perform energy recovery calculation for thermal plasma reactor. Typical gaseous products formed are rich in hydrogen and carbon monoxide, with some lower hydrocarbons (like methane). The reactions which take pace during the pyrolysis of simulated medical waste for cotton(cellulose) and plastic (polyethylene) are approximated as:

$$C_6H_{10}O_5 + heat \Rightarrow CH_4 + 2CO + 3H_2O + 3C \tag{3.10}$$

$$[-CH_2 - CH_2-]_n + H_2 + heat \Rightarrow xCH_4 + yH_2 + zCO \tag{3.11}$$

In several studies, wood pyrolysis models have been described from numerical analysis point of view. Babu et al. [49] present a generalized model for pyrolysis of biomass particle by considering combined effects of variable properties, heat convection, conduction and radiation,volatiles and gas transport by diffusion and convection and momentum transfer. Papadikis et al. [50] present CFD modeling results of the fast pyrolysis of an in-flight cellulosic particle subjected to convective heat transfer, incorporating thermal degradation of cellulose to char with simultaneous evolution of gases and vapors from discrete cellulosic particles. Sand et al. [51] performed numerical investigation of the transport and pyrolysis in the interior and surrounding of dry and wet wood log.

Generally reaction mechanism of biomass pyrolysis is described in terms of groups, by combining light product gases (CO,H_2 etc.) into just *gas* and heavy

hydrocarbons as *tar* and solid residue as *char*. Different classes of mechanisms are proposed for pyrolysis of wood and other cellulosic materials in [4]. One of the more sophisticated ways to model the pyrolysis of wood is to apply a mechanism involving two steps, a primary and a secondary pyrolysis step as follows [51]: 3.6.2.1. *

First Step

$$Wood \rightarrow Gas \tag{3.12}$$

$$Wood \rightarrow Tar \tag{3.13}$$

$$Wood \rightarrow Char \tag{3.14}$$

3.6.2.2. *

Second Step

$$Tar \rightarrow Gas \tag{3.15}$$

$$Tar \rightarrow Char \tag{3.16}$$

After pyrolysis gases are released from the wood or solid waste , they react with each other or with oxygen (if available) in homogeneous gas phase reactions. Also, produced char can react with pyrolysis gases and oxygen (if available).

The following simplified chemical conversion formulae describe these reactions [41, 52, 53]:

$$C(s) + H_2O = CO + H_2 \tag{3.17}$$

$$C(s) + CO_2 = 2CO \tag{3.18}$$

$$C(s) + 2H_2 = CH_4 \tag{3.19}$$

$$C(s) + O_2 = CO_2 \tag{3.20}$$

$$2C(s) + O_2 = 2CO \tag{3.21}$$

$$CH_4 + H_2O = CO + 3H_2 \tag{3.22}$$

$$CH_4 + 2O_2 = CO_2 + 2H_2O \tag{3.23}$$

$$CO + H_2O = CO_2 + H_2 \tag{3.24}$$

$$CO + 0.5O_2 = CO_2 \tag{3.25}$$

3.6.3 Kinetics

A simple kinetic model is used in order to predict the reaction rate for wide range of operating conditions and various types of wastes. The simplified approaches describe pyrolysis rates by Arrhenius reaction schemes. The reaction kinetic rate is expressed in Arrhenius fashion as

$$k = A \exp(-E_a/RT) \tag{3.26}$$

where k is reaction kinetic rate (s^{-1}), A is pre-exponential factor (s^{-1}), E_a (J/mol) is activation energy, R is the universal gas constant (J/mol-K) and T is the temperature (K).

One-step global schemes, such as given by reaction 3.6, lack any data about reaction kinetics. Whereas, in case of two-stage semi-global reactions, give by 3.12 - 3.16, there is a considerable diversity in the values of kinetic data in the literature [49–51]. The values used by Sand et al. [51], for numerical prediction of the transport and pyrolysis in the in the interior and surrounding of dry and wet wood log, are given in Table 3.4.

Table 3.4
Pyrolysis rates for wood log [51].

Mechanism	Rate(s^{-1})
Wood → Gas	$1.52E+07 \exp(-139.2/RT)$
Wood → Tar	$5.85E+06 \exp(-119.2/RT)$
Wood → Char	$2.98E+03 \exp(-73.1/RT)$
Tar → Gas	$2.6E+06 \exp(-108/RT)$
Tar → Char	$1.0E+06 \exp(-108/RT)$

The major limitation of simplified approach of two-stage semi-global reaction scheme is that they can not predict the composition of product gases and do not

account for various components of the virgin biomass. The other method of one-step multi reaction schemes can be used to overcome these shortcomings. In this method, the process is modeled based on the functional groups, like CO, CH_4, CO_2, H_2O, tar, char etc. [53]. Authors Yan J. H. , Zhu H. M. and others [54,55] have studied pyrolysis of medical waste using thermogravimetric analyzer with Fourier transform infrared spectroscopy (TG-FTIR) and presented evolution of different volatile species, using functional group approach. The results of this study are used as inputs to a pyrolysis model, which is based on first-order kinetic expression with a Distributed Activation Energies Model (DAEM).

DAEM has been widely used to analyze the complex reactions. The model assumes that the evolution of a given product involves an infinite number of independent chemical reactions. Each reaction contributes to the formation of a product according to [55]:

$$\frac{dY_i}{dt} = -k_i Y_i \tag{3.27}$$

where Y_i refers to the unreacted mass fraction of species i in the initial material and k_i denotes the rate constant of the corresponding reaction. The rate constant k_i typically has Arrhenius form given by Eq. (3.26).

The kinetic parameters for absorbent cotton pyrolysis, required for DAEM approach are given Table 3.5. For more details about how to implement DAEM approach in the numerical calculations refer to [56].

Table 3.5
Kinetic parameters (k_0,E_0 and σ) for absorbent cotton pyrolysis [55].

Species	$T(K)$	$k_0(s^{-1})$	$E_0(kJmol^{-1})$	$\sigma(kJmol^{-1})$
CO	$586-713$	$1e+15$	188.5	4.2
CO_2	$586-713$	$1e+20$	248.0	5.2
H_2O	$586-713$	$1e+21$	260.5	1.2
Hydrocarbon	$586-713$	$1e+23$	289.0	8.0
Aldehyde	$586-713$	$1e+19$	237.5	3.3
Ketone	$586-713$	$1e+21$	262.0	4.5
Acid	$586-713$	$1e+20$	249.5	5.1

4. PLASMA THERMAL REACTOR

4.1 Plasma Thermal Destruction Recovery Reactor

In this work, Plasma Thermal Destruction Recovery ("PTDR") system is selected as a model reactor for numerical simulations. PTDR is a proprietary technology of PEAT International, a waste-to-resources company headquartered in Northbrook (Illinois) , for the treatment and recycling of a wide range of waste feedstocks, including: industrial, universal and medical waste. In 1992, it first opened the research and development facility using the plasma technology in Hunstville, Alabama. Today it has PTDR facilities in US Army -Lorton (Virginia) , Ankleshwar (India), NCKU-Tainan (Taiwan), and Fooyin University-Kaohsiung.

PEAT has three reactor systems with different capacities for waste treatment:

- **PTDR-100:** The PTDR-100 reactor is a 60 kilogram per hour (130 pounds per hour) system, aimed for small to medium-sized waste generators, like hospitals and small industrial facilities looking for on-site solutions to their solid waste management challenges.

- **PTDR-500:** The PTDR-500 is a 250 kilogram an hour (550 pounds per hour) system, ideal for medium-sized generators.

- **PTDR-1000:** The PTDR-1000 is a 25 to 30 metric tons-per-day system that supports centralized waste processing and waste-to-resources applications. PTDR-1000 systems are equipped and designed to handle a wide variety of waste streams: liquid, solid, organic and inorganic. While the reactor and torch system remains the same, PTDR-1000 systems may have more customized subsystems than the PTDR-100 systems to address a design-basis feedstock.

4.2 PTDR-100 Overview

As mentioned in the previous section, PTDR-100 reactor is a 60 kilogram per hour (130 pounds per hour) system, aimed for small to medium-sized waste generators, like hospitals and small industrial facilities looking for on-site solutions to their solid waste management challenges.

It uses the heat generated by a graphite plasma torch system in an oxygen starved (pyrolytic) environment to first, dissociate the molecules of organic portions of the waste, then depending on the composition of the waste stream, a controlled amount of oxygen can be added to reform the dissociated elements into a synthesis gas which, when utilized will result in pristine emissions. The system derives its energy from plasma torches, thus wastes with little or no calorific value can also be treated effectively and efficiently. It has several environmental and economical key features, as mentioned below.

Environmental

- No secondary pollution or by-products generated: all feedstock is 100% waste diversion, totally eliminating the need for landfill disposal and/or further processing.
- Emissions below 40 CFR part 60, subpart FFFF and/or 40 CFR part 60, subpart Ec (US EPA).
- Eliminates any future liabilities to the generators resulting from the use of outside collection, treatment and disposal services/facilities that are potentially unscrupulous.
- High volume (over 200 to 1) and weight (over 10 to 1) reductions.
- High Destruction and Removal Efficiencies (DRE's) of organic materials (greater than 99.99%).

- Independent laboratory tests (toxicity characteristic leaching procedure or "TCLP") have proven that the vitrified product does not leach and is totally benign and safe for any re-utilization.
- Provides alternative energy options (approximately 200,000 kcal/hr).
- Capability of meeting the real recycling requirements.

Operational

- 60 kg/hr capacity occupying less than 50 m^2.
- 24/7 operating capabilities.
- Fast heat-ups to operating temperatures 1000-1600 K and natural cool-downs, allowing the system to be turned on and off quickly without the need of extensive pre- and post-operational procedures.
- Automated process control allows the system to be operated by a single trained operator.
- Nearly all types of solid waste feedstock (organic, inorganic and/or heavy-metal constituents) can be processed simultaneously, thus minimizing the pre-processing, staging, sorting and management costs.

Economical

- Installed capital cost less that $0.09 per kg (10 year amortization).
- Operations and maintenance costs as low as $0.29 per kg including labor.
- System investment generates favorable net-present values with low payback periods, based on existing market prices, industry dynamics and metrics.

Waste Stream Flexibility

The PTDR-100 system can handle a wide variety of wast feedstocks including:

- Biomedical wastes, including infections, chemo, pathological.
- Universal and/or industrial waste streams such as batteries and electronic waste, solvents and sludges.
- Contaminated soils.
- Incinerator fly ash.
- Pharmaceutical waste.

Figure 4.1 shows the schematic diagram of PTDR-100 with various subsystems. Each system is equipped with the following subsystems:

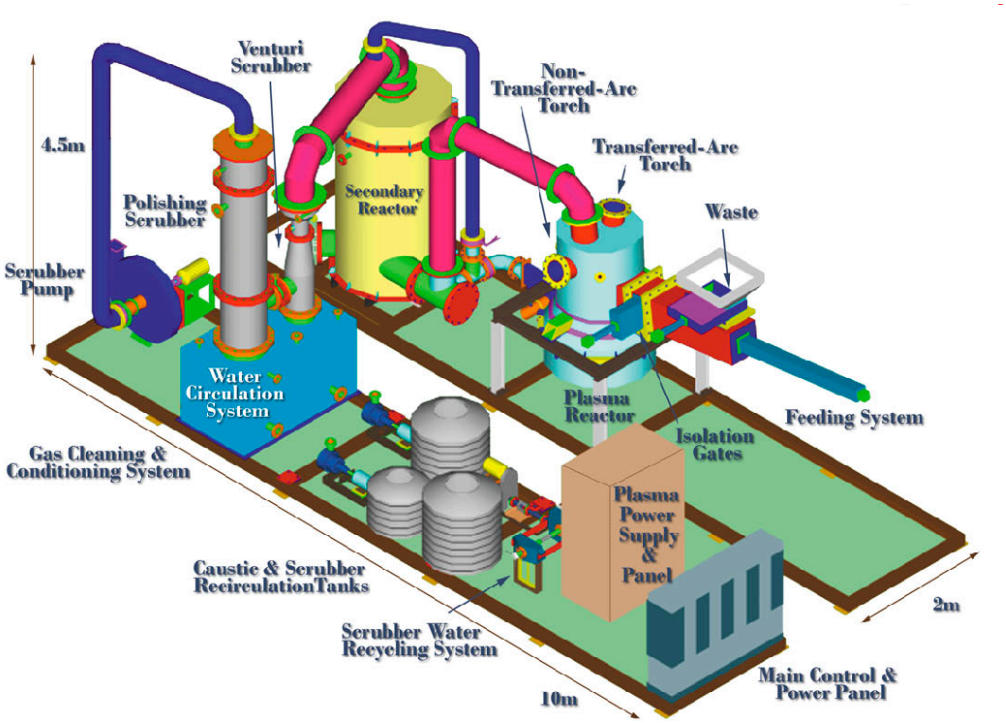

Figure 4.1. PEAT's PTDR100 Reactor.

- Feeding system
- Plasma torch
- Plasma reactor
- Secondary reaction chamber
- Gas conditioning and cleaning system
- ID fan
- Discharge stack
- Power Panel
- Process control system

The flow of operations, along with respective subsystem assigned for it, is explained next.

4.2.1 Plasma Torch

The 100 kW plasma generation system is utilized within the PTDR-100 system. There are two configurations of the reactor based on the plasma torch. In the first, non-transferred arc is utilized, while in the second, transferred arc is used. In reality both operating modes reflect transferred arc operation. During non-transferred arc operations, arc is transferred between two torches. The transferred arc torch, mounted at the top of the plasma reactor, moves up and down within the plasma reactor, while the non-transferred arc torch, mounted laterally and angled horizontally in the reactor, moves in and out along a radial direction. Due to these motions, torches are housed within a sealing and insulating assembly. This assembly insulates the torch body and ensures that its structural elements are maintained within a prescribed temperature range. This avoids the need of additional cooling, which would remove excess thermal energy from the torch and thereby reduce the electrical-to-thermal

efficiency. The entire plasma system has an electrical-to-thermal efficiency of greater than 80% and requires no pressurized external supply of carrier gas.

4.2.2 Solid Waste Feeder

Solid waste is lifted into a feed system consisting of two retractable, isolation gates. The system is programmed to assure one of the two gates remaining closed at all times. After the first door closes, nitrogen is used to pressurize the feeding chamber, to minimize the amount of air that can enter into the reactor with the feedstock. After the materials enter the feeding chamber, a hydraulic-powered ram feeder pushes the waste feedstock into the plasma reactor. The feeding system is designed to accommodate 30-gallon medical waste bags and 250 mm^3 boxes. The section of the feeder closest to the plasma reactor is refractory, lined to ensure the feeding chamber remains within a prescribed temperature limit, also to ensure that any plastic bags containing medical waste do not thermally degrade in the feeding chamber. A load cell monitors the quantity of feedstock being introduced into the feeding subsystem.

4.2.3 Plasma Reactor

The waste then enters the plasma reactor, made of mild steel and lined with refractory and insulation, where the high temperature created by the plasma torch dissociates the molecules that make up the waste into their elemental constituents. The plasma reactor allows for a residence time of 2.0 seconds based on a design basis gas flow.

Waste, when heated to a very high temperature in the controlled atmosphere of the reducing plasma reactor, undergoes predictable physical and chemical changes. This high temperature, over 1000 K, prevents the formation of complex organic molecules and breaks down organics into a gas. These primary molecules are stable above 1000 K . The organic elements of the waste combine with moisture and

oxygen inherent in the waste feedstock to produce a synthesis gas ("syngas"), comprised principally of carbon monoxide and hydrogen. The formation of dioxins or furans is impossible inside the plasma reactor due to the unique process features, including high uniform temperatures and a lack of excess oxygen within the system.

4.2.4 Secondary Reaction Chamber

The syngas is then processed further in a secondary reaction chamber, also made up of mild steel. Depending on the operating mode and the waste being processed, the syngas can be further conditioned to be used in one of several energy recovery options. If a syngas utilization system is not available, the gas is transformed to produce nitrogen, oxygen, carbon dioxide and water vapor. The residence time in this subsystem is approximately 3.0 seconds, depending on the waste being processed.

4.2.5 Gas Cleaning and Conditioning System

The resulting gas, at a temperature of approximately 1400 K, is then fed through a gas cleaning and conditioning system, where the gases are rapidly cooled to ensure that there is no potential for the generation or re-association of any undesired molecules, such as dioxins or furans. The gas is then cleaned to remove any entrained particulate matter and acid gases. The system consists of a venturi/packed bed scrubber. The scrubber also serves to remove excess moisture from the gas in conjunction with a cooling tower. A caustic solution is added to the recirculating water in the venturi scrubber to scrub the acid gases. Cooled water is recycled throughout the system.

4.2.6 Slag Remover

Any inorganic constituents in the waste are melted (vitrified) by the non-transferred arc torch and the graphite-lined plasma reactor bottom into an environmentally safe, leach resistant, vitrified matrix. The removal of the vitrified matrix

presents no hazards of any kind to personnel, requires no special tools and does not disrupt the operating process.

4.2.7 Process Control System

The PTDR-100 process is driven by proprietary, state-of-the-art instrumentation and a computerized control system. The Human Machine Interface (HMI) system is the process control system that provides a graphic-based visualization of the system control and monitoring system. The HMI communicates with the process logic control system, integrated within the PTDR-100. The control system obtains inputs from all of the PTDR-100 process subsystems to achieve total overall control of the system. Safety, interlocking features and emergency shut-down aspects specific to each subsystem are incorporated to assure safety features are not compromised.

While the operations can be monitored and controlled using the HMI system, the operator is also provided with a Supervisory Control And Date Acquisition (SCADA) system - a distributed measurement and control system, which includes hardware and software components.

Each subsystem has customized interface screens. The SCADA system monitors critical input and output parameters and prompts the operator to make appropriate adjustments (or makes automatic adjustments for critical safety-related conditions) to the waste feed rate, plasma reactor temperature, oxidant input (if required), and the gas cleaning and conditioning system to ensure that the system operates to meet prescribed environmental requirements. The SCADA system also records and logs all events for further assessment.

4.2.8 Day-to-day Operations

In terms of consumables, the PTDR-100 system requires electricity, water, auxiliary fuel (for the secondary reaction chamber), caustic (for the gas cleaning and

conditioning system) and plasma electrodes. Details of utilities and consumables are as follow:

- **LPG or Natural gas:** approximately 500 liters/hr during pre-heating (one hour) and approximately 1.5 liters/hr during normal operations.
- **Electrical:** maximum consumption 130 kW, 380-415 Volts, 3-Phase, during normal operations the system consumes 40-75 kW, of which, 2-50 kW is from the plasma torch and 25 kW is for balance of plant systems.
- **Water:** 12 liters/min.

Approximately 60 to 90 minutes are required to reach the operational bulk temperatures in the plasma reactor and the system cools down naturally after torch shutdown (and can be restarted at any time during the cool down process). During normal operations, at the start of each feeding campaign, or at the end of an operating shift, the plasma reactor may contain some non-organic residues. The transferred arc torch is operated initially, which pre-heats the plasma reactor and helps to vitrify any leftover residue. After all the residue has been vitrified, it is removed via a simple tapping process. The entire vitrification/tapping process takes approximately 45 to 60 minutes.

The replacement electrode sections for the plasma generation system are approximately 330 mm in length and can be continuously attached to the back of the existing electrode from the outside of the reactor. There is no need to remove system components during electrode replacement activities, thus there is little downtime. The replacement of bottom electrode is likely needed on a once-a-month basis.

5. REVIEW OF SOLID WASTE PYROLYSIS NUMERICAL MODELING

Despite recent progress in CFD modeling techniques, numerical modeling of plasma assisted solid waste pyrolysis faces significant challenges, because of inherent complexity of the process. It is a multi-physics process involving electromagnetism (plasma), multi-phase (solid,liquid,gas) flow, heat transfer, species transport, homogeneous and heterogeneous chemical reactions (vaporization, devolatilization, char gasification, gas phase reactions) along with turbulence and radiation phenomena. Numerical modeling of each of these phenomena individually is in itself a challenge and combining effects of all makes it more difficult. Hence, the key point is to simplify the complex process for numerical simulation model. Literature lacks any significant work on numerical modeling of plasma assisted pyrolysis of solid waste. However, many studies have been performed on the biomass pyrolysis.

Currently there are two approaches for the numerical calculation of solid-fluid reacting flows : the Euler-Lagrange approach and the Euler-Euler approach. In the Euler-Lagrange approach fluid phase is treated as a continuum by solving the time-averaged Navier-Stokes equations, while the dispersed phase is solved by tracking a large number of particles, bubbles, or droplets through the calculated flow field. The dispersed phase can exchange momentum, mass and energy with the fluid phase. In the Euler-Euler approach, the different phases are treated mathematically as interpenetrating continua. Since the volume of a phase cannot be occupied by the other phases, the concept of phasic volume fraction is used. These volume fractions are assumed to be continuous functions of space and time and their sum is equal to one. Conservation equations for each phase are derived to obtain a set of equations, which have similar structure for all phases. These equations are closed by providing con-

stitutive relations that are obtained from empirical information, or , in the case of granular flows, by application of kinetic theory [57].

In many biomass pyrolysis applications, biomass solid is fragmented into small particles before it enters the reaction chamber. Hence, it is suitable to use Euler-Lagrange approach for tracking biomass particles through the gas phase in reaction chamber. Calculation of reacting biomass particle trajectory involves formulation, that includes [57]:

- the discrete phase inertia, hydrodynamic drag and the force of gravity
- prediction of the effects of turbulence on the dispersion of particles due to turbulent eddies present in the continuous phase
- heating/cooling of discrete phase
- vaporization, volatile evolution and char combustion
- coupling of the continuous phase flow field to the discrete phase calculations

Instead of modeling complete coupling, between discrete phase and continuous gas phase, only modeling of processes taking place inside a stationary,reacting biomass particle, can be useful to understand the behavior of it. Babu and Chaurasia [49] present 1-D models to simulate chemical process of pyrolysis, incorporating effects of an unsteady state, variable property, heat convection, conduction and radiation, volatiles and gas transport by diffusion and convection and momentum transfer. The objective is to model single stationary biomass particle undergoing pyrolysis and the effects of heat transfer, gas flow and reactions are considered. Vaporization and effects of particle shrinkage are neglected. A finite difference pure implicit scheme utilizing a Tri-Diagonal Matrix Algorithm (TDMA) is employed for solving the heat transfer and mass transfer model equations. A Runge-Kutta fourth order method is used for chemical kinetics model equations. Simulations are performed considering different geometries of equivalent radius, ranging from 0.0001 to 0.017 m and temperatures ranging from 303 to 2800 K. The models are validated with experimental data

and are utilized to investigate the influence of particle size, particle shape, product distribution, conversion time and heat of reaction.

Many times the objective of numerical modeling is to understand the particle movement and product gas mixing inside the reactor. The detail modeling of processes occurring inside each particle can be computationally expensive and complex. Papadikis et al. [50] present CFD modeling of the fast pyrolysis of an in-flight cellulosic particle subjected to convective heat transfer. The commercial CFD code FLUENT is used for numerical simulation. The pyrolysis of a freely moving cellulosic particle inside a continuously fed fluid bed reactor is modeled. The Lagrangian approach is adopted for the particle tracking, while the flow of the inert gas is treated with the standard Eulerian method. The temperature is assumed to be uniform inside the particle. Two cases of particle heating are modeled. In the first case, infinitely fast external heat transfer rate (IFEHTR) is assumed. In IFEHTR, the particle temperature rises instantaneously to the reactor temperature and the reaction mechanism is instantaneously initiated. In the second case, Ranz-Marshall correlation is employed to model heating of particle. For simplification, the heat of reaction, particle fusion and particle evaporation are assumed to be zero. The reaction kinetics are modeled using the Broido-Shafizadeh scheme. It is found that different heat transfer conditions result in different particle trajectory and different pyrolysis product yields, which are highly dependent on the residence time and the pyrolysis products itself. The significance of this model is that, in contrast with single particle models, such as [49], the discrete phase modeling of the biomass pyrolysis can predict the particle position inside the reactor, its residence time as well as the residence time of the gases produced inside the reactor.

In another similar study Backreedy et al. [58] present a CFD modeling study to examine the co-firing of pulverised coal and biomass. Discrete Phase model of commercial code FLUENT is used for Euler-Lagrangian approach. It is assumed that many aspects of coal and biomass combustion process are common, and that the key sub-models are the same as for coal, i.e., those applicable to drying, devolatilisation,

and volatile and char combustion, together with the behavior of special components such as ash and volatile metals. Along with conductive and convective heat transfer, radiation is considered through P-1 radiation model. Also the RNG k-ϵ turbulence model is implemented to account for swirling flow. The effects of the wood particle size and shape on the burnout of combined wood and coal char are investigated. Also, different devolatilisation and char combustion rate constants for the biomass component in the blend are investigated.

However the Euler-Lagrangian model assumes that the second phase , i.e. discrete phase, is sufficiently dilute that particle-particle interactions and effects of the particle volume fraction on the gas phase are negligible. This implies that discrete phase must be present at a fairly low volume fraction, usually less than 10-12% [57]. In many plasma assisted solid waste management systems, like PEAT's PTDR100, solid waste is compacted in cubical shapes and then fed into the reactor. Size of these compacted cubes can be as large as 400 mm^3. Also in case of fluidized bed systems, particle-particle interaction is significant and can not be neglected. These modeling needs can not be addressed using Euler-Lagrangian approach because of its limitations. Hence, the other option of Euler-Euler approach can be considered, which treats solid phase also as continua and has no set limitations on the size of particles and its volume fractions.

Ravelli et al. [5] have done significant study on application of Euler-Euler approach for modeling of bubbling fluidized bed combustion (FBC) in waste-to-energy plants. In their investigations, it is found that FBCs have been modeled mainly with zero-dimensional or one-dimensional models. Whereas, multi-dimensional models of chemically reactive fluidized beds, using Euler-Euler approach, are still lacking in the literature, since the bed hydrodynamics and combustion reactions are troublesome issues to deal with together in more than one co-ordinate. Although the works concerning multi-dimensional, multi-phase simulation of fluidized beds exist, but none of them takes chemical reactions into account. Because of these difficulties in using Euler-Euler approach for modeling heterogeneous reactions along with hydrodynam-

ics, authors take simplifying majors. The fluidized bed is neglected from calculations, instead heat and mass fluxes from the bed are computed knowing the chemical composition of the waste in the bed. These fluxes are then used as boundary conditions for fluid flow simulations in the freeboard, FLUENT. Also any particulate matter entering freeboard from the bed is modeled using Euler-Lagrangian approach, because it satisfies the requirements for use of discrete phase model.

Papadikis et al., in their studies [50, 50], present use of Euler-Euler approach for CFD modeling of the fast pyrolysis of biomass in fluidised bed reactors. Fluidised sand is used in the reactor for improving the heat transfer to the biomass particle. Euler-Euler approach is used to simulate the behavior of the sand. Whereas biomass particle is simulated using discrete phase model. FLUENT is used as the modeling framework of the simulations. It can be noticed that, in this study also, Euler-Euler approach is used only for non-reacting part of the reactor, while reacting particles are treated using Lagrangian approach.

Porous media model is another approach to model solid waste transport, along with reactions. As solid waste undergoes various pyrolysis reactions, the product gases escape through pores already existing inside the compacted waste and result in more pores. This behavior of solid block of waste can be described using porous media model. In numerical simulation, the porous media model is nothing more than an added momentum sink in the governing momentum equations [57]. Hence, the reactions can be modeled using usual species transport model, similar to homogeneous reactions. Sand et al. [51] employ porous media approach for numerical prediction of the transport and pyrolysis in the interior and surrounding of dry and wet wood log. The stationary cylindrical wood log is modeled as porous zone, whose permeability is a function of wood and char species concentration. The model incorporates effects of flow inside and outside of porous wood log, convective, conductive and radiative heat transfer, a two-step pyrolysis reaction scheme is used to model the conversion from wood to tar, gas and char. The results show that, wood log acts as flow resistance and the product gases are diffused and convected through the porous zone.

Although porous media model is a viable substitute for Euler-Euler approach to model transport of solid waste along with pyrolysis reactions, it has issues regarding numerical stability. Though it is shown that stationary wood log pyrolysis can be modeled successfully using porous media approach, modeling moving porous zone poses significant numerical stability challenges. In out attempts, it is observed that very small time steps, which can be unphysical, must be used to model transport of porous zone through fluid. The cause of this can be attributed to very large jump in the momentum source/sink terms at the porous media interface, which is a function of solid species concentration.

Considering limitations of Euler-Lagrangian, Euler-Euler and Porous media approaches and costs involved in comprehensive CFD modeling of complete industrial level reactor, some key simplifying assumptions must be made. For the studies aiming to understand the mixing of product gases, recirculation zones, pathlines inside the reactor, assumptions like instantaneous pyrolysis reactions at the inlet and approximating solid flow using species transport can be made with considerable caution. Similar approach is followed by Fiedler et al. [59] in their work of numerical investigations of a plasma reactor for the thermal destruction of medical waste using a model substance. Three-dimensional CFD modeling of the gaseous phase in the thermal plasma reactor is carried out to investigate the experimentally observed phenomena, with the objective of improving the process. Due to high temperature zones created inside reactor, by applying plasma torch, instantaneous solid waste pyrolysis at the inlet is assumed. As one of the objectives is to understand temperature field inside the reactor, the heat of reactions is taken care by including appropriate source terms for energy equations. The commercial CFD code Flotran is employed. The results are validated qualitatively using experimental data and information about temperature, velocity and residence time distributions are obtained. The knowledge of these parameters allows conclusions to be drawn on the process flow, conversion rate and the utilization of high enthalpy plasma gas.

6. DESCRIPTION OF NUMERICAL MODEL

For any chemical reactor, mixing and residence times of gas species are critical design parameters for effectiveness and efficiency of the reactor. Destruction of toxic components of medical waste and restricting production of pollutant gas species such as CO_2, is very critical in the operation of thermal plasma reactor. If the objective is energy recovery, sufficient amount of synthesis gas (i.e. CO and H_2) must be produced. Insufficient mixing and small residence times may result in incomplete gasification of solid waste and higher hydrocarbons may escape the reactor without further cracking. Hence, it is important to design thermal plasma reactor in such a way that sufficient mixing and residence times are achieved. CFD modeling can play an important role in evaluating reactor's performance.

In this work, numerical model is developed for simulating flow inside the PTDR-100 reactor, incorporating the effects of plasma, turbulence, heat transfer, species transport and reactions. Using this numerical model different geometries and configurations of PTDR-100 reactor are compared on the basis of mixing efficiencies, residence times and species evolution.

As explained in the review, modeling solid-gas coupled flow, along with reactions, is a challenging problem and coexistence of so many complex phenomena makes the comprehensive numerical simulation of thermal plasma reactor an unreachable target. As a consequence, key approximations are made based on the experimental observations. These approximations are as follows:

- For simplicity detailed modeling of plasma torch is avoided by appropriate approximations at torch inlet. In case of PTDR-100 configuration, in which solid waste is directly interacting with plasma jet, plasma torch is modeled by using analytical model of [1]. Whereas, in the configuration where waste does not

come directly in contact with plasma jet, plasma torch is approximated by air flow inlet with experimentally found temperature and mass flow rate.

- Because of limitations of available numerical models to simulate reacting solid-gas flow, solid waste is approximated by gas phase with appropriate species concentration. This approximation can be justified based on the experimental observation of PTDR-100. It is observed that, because of very high temperatures (2000K) inside reactor, 10-15% of the solid waste gasifies as soon as it enters the reactor, remaining solid falls down to the bottom and gasifies there. Hence, only 10% of total required mass flow rate is assigned at the solid waste inlet and remaining 90% is added as source terms for solid waste species at the bottom of the reactor.

The full-scale 3-D PTDR-100 reactor model is implemented using commercial CFD code FLUENT 6.3 and is mainly concerned with the species transport approach to model gasification and gas phase reactions. Different geometries and configurations of PTDR-100 reactor are simulated for comparisons, in terms of mixing efficiency and residence times. The predicted data is in good agreement with experimental observations. The ultimate aim is to demonstrate that a 3-D CFD model can be used to evaluate performance of thermal plasma reactor and to perform critical design analysis.

6.1 Geometry and Grid

Fig 6.1 shows four different configurations of PTDR-100. First generation of PTDR-100 (called as generation 1), is characterized by direct interaction of plasma jet and solid waste. As shown in Fig. 6.1(a) two plasma torches are employed, one is located at the top and other is located on the circumferential wall of the reactor. Reactor has maximum diameter of 1300 mm at the bottom and minimum diameter of 1000 mm at the top. Total height of the reactor is 1360 mm. The solid waste inlet

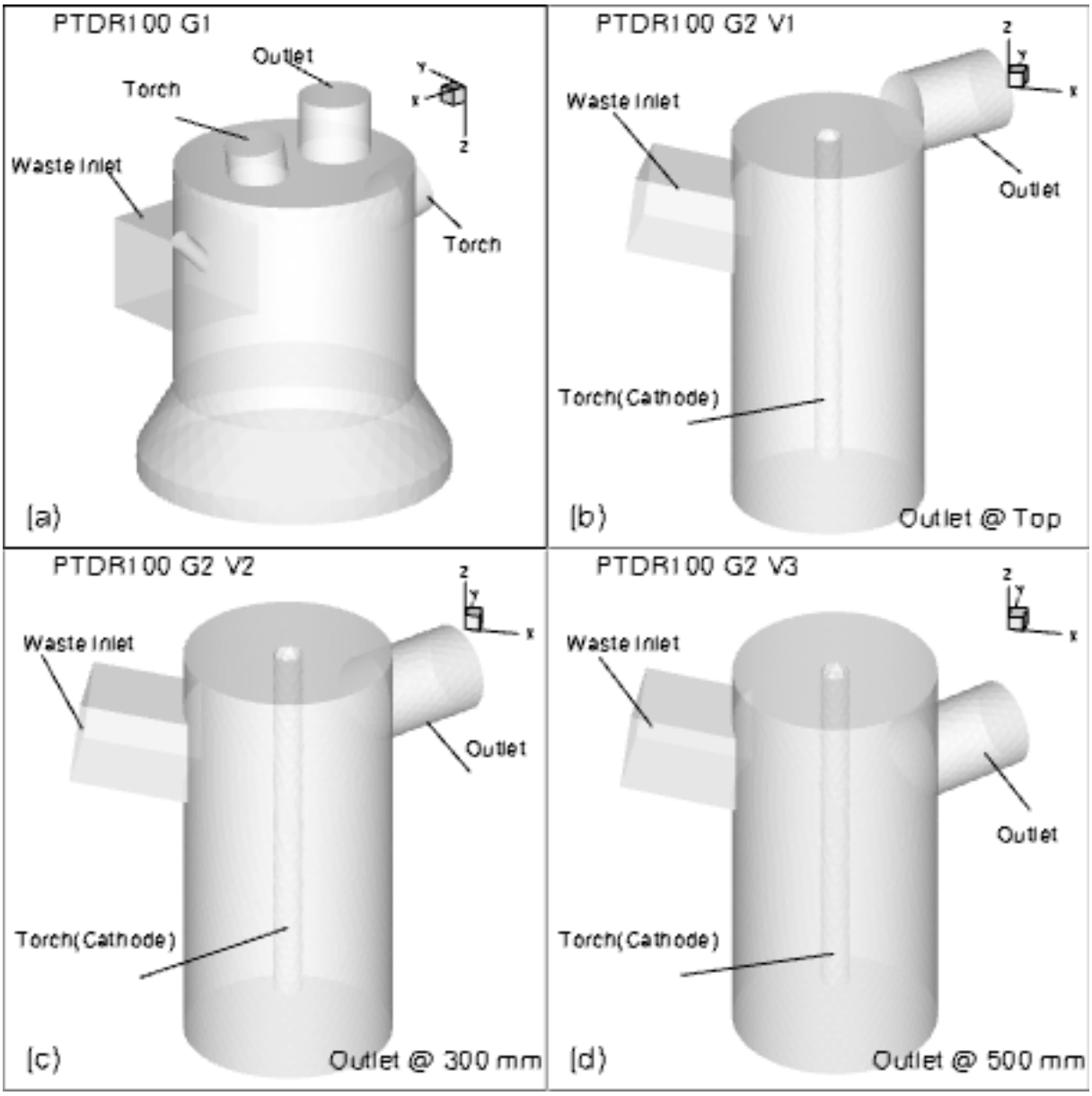

Figure 6.1. PTDR-100 Geometry (a)Generation 1 (b) Generation 2 version 1 (c) Generation 2 version 2 (d) Generation 2 version 3.

has cross sectional area of 300 $\times$ 300 mm^2 and is located about 860 mm from the bottom surface. Outlet has diameter of 300 mm and is located at the top surface.

In the second configuration of PTDR-100 (here, called as generation 2), solid waste does not directly interact with the plasma jet. Instead, transferred plasma arc is struck at the bottom of the reactor between graphite cathode, which runs down axially from top to the bottom as shown in the Fig. 6.1 (b)-(d), and anode. Anode is a graphite electrode of rectangular shape of cross section 150 $\times$ 150 mm^2 and cathode is 100 mm diameter cylinder. The plasma arc is separated from main section of the reactor by Silicon-Carbide tile assembly. As main objective of the study is to analyze flow inside the reactor, plasma assembly is neglected in the simulation and it is approximated by hot air inlet through the cathode. The height of the reactor is 1455 mm and diameter is about 700 mm. Solid waste has cross section of 300 $\times$ 300 mm^2 and it is inclined at 7^o to the horizontal. Outlet has diameter of 300 mm and an angle between solid waste inlet location and outlet is about 135^o. Three different geometries, depending on the outlet location height, are considered for this configuration of PTDR-100. In the first version, outlet is positioned near the top surface of the reactor. In the second, it is located at 300 mm from the top and in the third, outlet is 500 mm from the top.

Mesh generated for each geometry is presented in Fig. 6.2. Unstructured grid has been applied for each reactor geometry. The number of elements and nodes used in each reactor mesh are given Table 6.1 .The main objective here is to perform qualitative comparisons, the requirement of the fine mesh just to achieve high calculation accuracy was disagreed with the need to limit computation time. However, heat transfer modeling may be affected by grid features. Hence, finer mesh is used in the regions, where most of the solid waste gasification takes place. As shown, the mesh has been thickened by factor of two in the critical regions of solid waste inlet and at reactor bottom, where slag is accumulated and most of the gasification occurs.

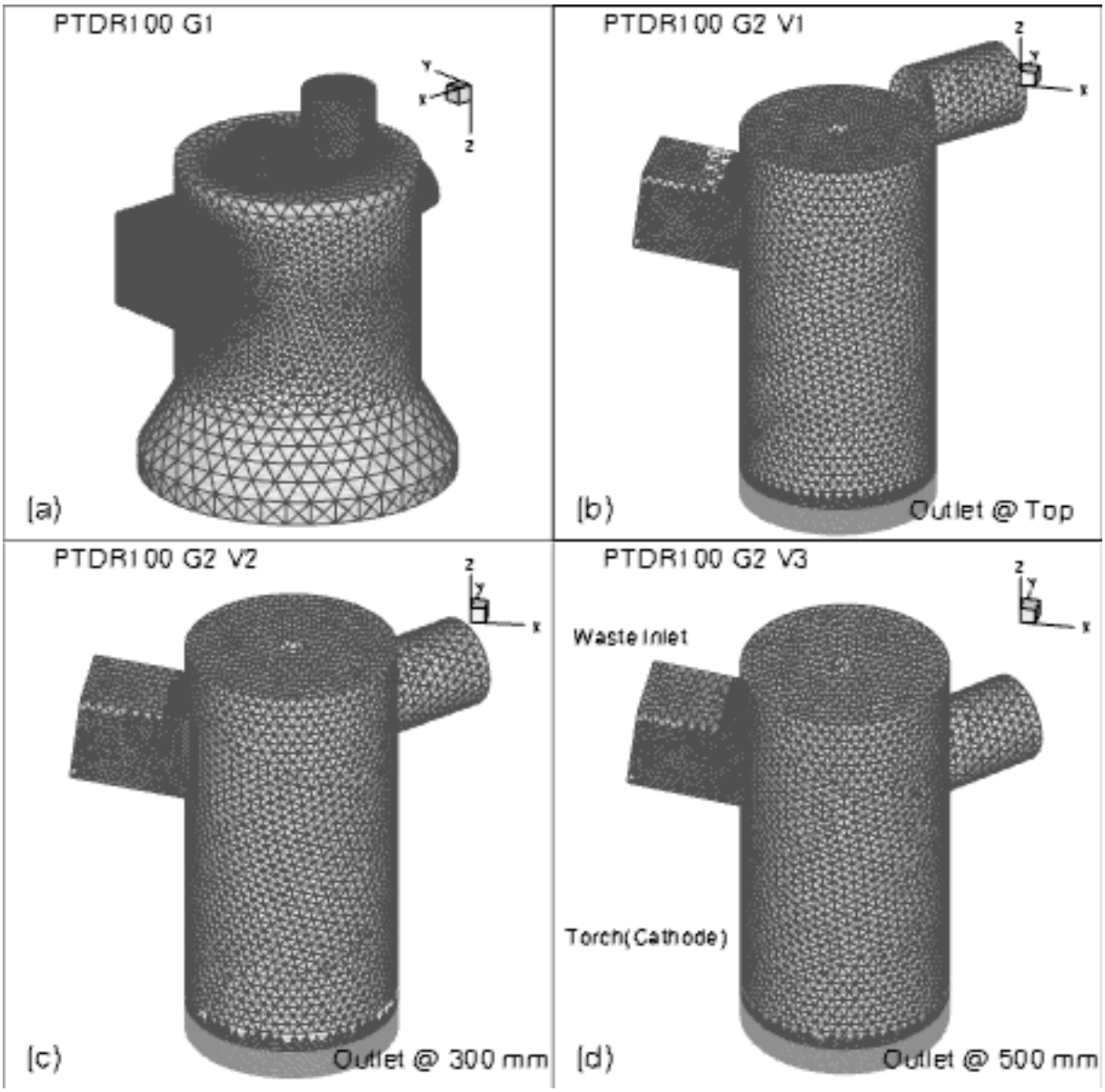

Figure 6.2. PTDR-100 Mesh.

Table 6.1
Mesh information.

Geometry	Cells	Faces	Nodes
G 1	167194	351619	36871
G 2, V1	147633	304572	29398
G 2, V2	173983	357615	33961
G 2, V3	164409	338446	32364

6.2 Numerical Model

Finding exact solution of governing equations and resolving all the time and length scales in multi-dimensional, turbulent, reacting computations is not possible. Hence, CFD model makes fundamental assumptions to allow calculation of spatial and temporal variations of velocity, pressure, temperature, particle trajectories, species concentrations etc. In this work, CFD model is composed of incompressible, steady-state form of governing equations of mass, momentum and energy, along with sub-models to account for turbulence, species transport and reactions, and radiation heat transfer. Summary of physical models used in this work is given in Table 6.2.

6.2.1 Discretization Method

Discretization is the process of approximating governing partial differential equations, such as Navier-Stokes equations, by algebraic expressions for obtaining numerical solution. FLUENT derives discretized equations from integral form of the conservation equations. This approach is known as control-volume method. The control volume technique consists of integrating the transport equation about each control volume, yielding a discrete equation that expresses the conservation law on a control-volume basis. By default, discrete values of the scalar are stored at the cell centers. However, face values of scalars are required for the convection terms in the

Table 6.2
Summary of Physical and Numerical Models Employed.

Phenomena	Numerical Model
Basic Fluid Flow	Steady, Incompressible Navier-Stokes
Turbulence	Standard 2-eqn k-ϵ
Species	Species Transport
Reactions	Eddy-Dissipation for Gaseous Reactions and Arrhenius Expression for Waste Gasification
Radiation	P-1 Model with Domain Based WSGGM Absorption Coefficient
Discretization	Finite-Volume with Second Order Upwind Scheme (except for Pressure, Standard Scheme)
Pressure-Velocity Coupling	SIMPLE
Solver	Pressure Based Segregated Solver with Algebraic Multigrid (AMG) Scheme

governing equations and must be interpolated from the cell center values. This is accomplished by using an upwind scheme. For the purpose of achieving higher order accuracy the second-order upwind scheme is employed in this work for all the scalar quantities, except for pressure the standard method is chosen [57].

6.2.2 Solution Algorithm

The pressure-based segregated algorithm is employed to solve the discretized governing equations. In pressure based method, the constraint of mass conservation of the velocity field is achieved by solving a pressure equation. The pressure equation is derived from the continuity and the momentum equations, in such a way that the velocity field, corrected by the pressure, satisfies the continuity. Since the governing equations are nonlinear and coupled to one another, the solution process involves iterations, wherein the entire set of governing equations is solved repeatedly until the solution converges.

The segregated solver solves individual governing equations for the solution variables one after another sequentially. Each governing equation is decoupled from other equations while being solved. Each iteration is carried out in following steps:

1. Update fluid properties based on the current solution. In case of first iteration, the fluid properties are updated according to initial approximation.

2. Solve the momentum equations, one after another, using the recently updated values of pressure and face mass fluxes.

3. To make sure velocity obtained in the previous step satisfies the continuity equation, solve the pressure correction equation using the recently obtained velocity field and the mass-flux. The pressure-velocity coupling is achieved by by the SIMPLE algorithm.

4. Correct face mass fluxes, pressure, and the velocity field using the pressure correction obtained in the previous step.

5. Solve the equations for additional scalars, such as turbulent quantities, species, energy, radiation intensity etc., using the current values of the solution variables.

6. Finally, check for the convergence of the equations.

Implicit scheme is used to linearize the conservation equations with respect to the dependent variable. Implicit solution of the linearized equations on unstructured grid is complicated. An Algebraic Multigrid (AMG) scheme is used to accelerate the convergence of the solver by computing corrections on a series of coarse grid levels. The use of this multigrid scheme can greatly reduce the number of iterations and the CPU time, required to obtain a converged solution [57].

6.2.3 Sub-Models

Although, Navier-Stokes equations describe the basic fluid flow, using conservation laws of mass, momentum and energy, they have a limited amount of applications in real thermal reactor process. Hence, additional physical submodels are required to represent the physical process. The important additional models used in this work include turbulence models, species transport and radiation heat transfer models. 6.2.3.1. Turbulence Modeling

The Reynolds-averaged approach is adopted for turbulence modeling. The Reynolds-averaged Navier-Stokes (RANS) equations represent transport equations for the mean flow quantities only. This introduces unclosed Reynolds stress terms in the time-averaged conservation equations and need to be modeled for turbulence closure.

The standard k-ϵ model is employed for modeling the turbulence. It is a semi-empirical model based on transport equations for the turbulence kinetic energy (k) and its dissipation rate (ϵ). It assumes that the flow is fully turbulent, and the effects of molecular viscosity are negligible. Standard k-ϵ is the simplest turbulence model, which allows the turbulent velocity and length scales to be independently determined. It is popular in industrial flow and heat transfer simulations for its robustness, economy, and reasonable accuracy for a wide range of turbulent flows. The default values for various model constants are used in this work [57].

6.2.3.2. Species Transport and Reactions

The mixing and transport of chemical species can be modeled by solving conservation equations of convection, diffusion, and reacting sources for each component species. Multiple simultaneous chemical reactions can be modeled, with reactions occurring in the bulk phase. The solid waste transport and gasification reactions are modeled using FLUENT's species transport and the eddy-dissipation formulation.

In species transport model, the local mass fraction of each species, Y_i, is predicted through the solution of a convection-diffusion equation for the ith species. This conservation equation takes the following general form:

$$\frac{\partial(\rho Y_i)}{\partial t} + \nabla \cdot (\rho \vec{v} Y_i) = -\nabla \cdot \vec{J}_i + R_i + S_i \tag{6.1}$$

where ρ is fluid density, $\vec{v}$ is velocity, R_i is the net rate of production of species i by chemical reaction and S_i is the rate of creation by addition from the dispersed phase plus any user-defiined sources, $\vec{J}_i$ is the diffusion flux. In turbulent flows, the mass diffusion flux is solved in the following form:

$$\vec{J}_i = -\left(\rho D_{i,m} + \frac{\mu_t}{Sc_t}\right) \nabla Y_i \tag{6.2}$$

where $D_{i,m}$ is the diffusion coefficient for species i in the mixture, Sc_t is the turbulent Schmidt number ($\frac{\mu_t}{\rho D_t}$ where μ_t is the turbulent viscosity and D_t is the turbulent diffusivity). Eq. (6.1) is solved for $N-1$ species and N^{th} mass fraction is determined as one minus the sum of the $N-1$ solved mass fractions.

Due to high temperatures in thermal plasma reactor, gas phase chemical reactions are very fast and the overall rate of reaction is controlled by turbulent mixing. In such cases, the reaction is said to be mixing-limited, and the complex and unknown chemical kinetic rates of gas phase reactions can be safely neglected. Hence, eddy-dissipation model for gas phase reactions is appropriate. In this formulation, the chemical reaction rate is governed by the large-eddy mixing time scale, $\frac{k}{\epsilon}$.

The effects of enthalpy transport due to species diffusion and energy sources due to reactions $S_{h,rxn}$ are added to the energy equation. These sources are given as:

- Enthalpy transport due to species diffusion

$$\nabla \cdot \left(\sum_{i=1}^{n} h_i \vec{J}_i \right) \tag{6.3}$$

- Reaction Energy sources

$$S_{h,rxn} = -\sum_{j} \frac{h_i^0}{M_i} R_i \tag{6.4}$$

where h_i is specific enthalpy of species i, h_i^0 is the enthalpy of formation of species i, R_i is the volumetric rate of creation of species i.

6.2.3.3. Radiation Heat Transfer

In thermal plasma processes, due to high temperatures radiation is the dominant energy transport method. In a reactor fed by solid waste, radiation includes contributions from both particulate (C_s) and gas, mainly CO_2 and H_2O. Therefore, the radiative heat transfer model must comprise conservation equation for radiant energy and radiative properties of gases. The choice of radiation transfer model depends on the optical thickness. As for thermal plasma reactor optical thickness is greater than unity, the P-1 model is appropriate [5].

The P-1 radiation model is the simplest case of the more general P-N model, which is based on the expansion of the radiation intensity into orthogonal series of harmonics. FLUENT solves the transport equation for the incident radiation, given as:

$$\nabla \cdot (\Gamma \nabla G) - aG + 4a\sigma T^4 = S_G \tag{6.5}$$

where, a is the absorption coefficient, σ is the Stefan-Boltzmannn constant, G is the incident radiation, T is the temperature, S_G is a user-defined radiation source. And Γ is given by

$$\Gamma = \frac{1}{(3(a + \sigma_s) - C\sigma_s)} \tag{6.6}$$

where σ_s is the scattering coefficient and C is the linear-anisotropic phase function coefficient. So the radiation flux term q_r used in energy equation is :

$$q_r = -\Gamma \nabla G \tag{6.7}$$

The P-1 model works reasonably well for reactive flow applications and is easy to solve with little CPU demands. In addition, the P-1 model can easily be applied to complicated geometries with curvilinear co-ordinates. The model includes the effects of scattering. The limitations of this model are: it assumes that all surfaces are diffuse; it assumes gray radiation; there may be a loss of accuracy, depending on the complexity of the geometry, if the optical thickness is small; it tends to over-predict radiative fluxes from localized heat sources or sinks [57].

In thermal plasma reactor, water vapor and carbon dioxide are the major absorbers/emitters of radiant energy. Absorption and emission by gas species are important only in specific wavelength regions and exact spectral description is time consuming calculation procedure. Hence, wide-band models are much easier to use and widespread [5]. FLUENT allows to use a composition-dependent absorption coefficient for CO_2 and H_2O mixtures using the Weighted-Sum-of-Gray-Gases Model (WSGGM). It is a reasonable compromise between the oversimplified gray gas model and a complete model which takes into account particular absorption bands. Domain based WSGGM is used to define the absorption coefficient of the gas and scattering effects are completely neglected [57].

6.3 Input Data and Boundary Conditions

As explained before, gasification of solid waste is very complex process. The comprehensive kinetic model of thermo-chemical conversion of waste is not available at the moment. Hence, key approximations are made as per experimental observations. Based on the composition of medical waste and product gas, the species included in the model are: Cellulose ($C_6H_{10}O_5$), H_2O,CH_4,CO,CO_2,H_2,C_s,O_2,N_2.The medical waste used in PTDR-100 is simulated by cotton. The gasification of solid waste is approximated by the reaction [14]:

$$C_6H_{10}O_5 + heat \Rightarrow CH_4 + 2CO + 3H_2O + 3C \tag{6.8}$$

After gasification, product gas species react with each other and limited amount of oxygen present in the reactor. The gas phase reactions and char gasification are approximated by considering following reactions:

$$C(s) + H_2O = CO + H_2 \tag{6.9}$$

$$C(s) + CO_2 = 2CO \tag{6.10}$$

$$C(s) + 0.5O_2 = CO \tag{6.11}$$

$$C(s) + O_2 = CO_2 \tag{6.12}$$

$$CH_4 + H_2O = CO + 3H_2 \tag{6.13}$$

$$CH_4 + 2O_2 = CO_2 + 2H_2O \tag{6.14}$$

$$CO + H_2O = CO_2 + H_2 \tag{6.15}$$

$$CO + 0.5O_2 = CO_2 \tag{6.16}$$

The functional group approach is employed for kinetics of gasification reaction and eddy-dissipation formulation is used for gas phase reactions. Only two functional groups are considered, CH_4 and CO. Moisture in the waste is assumed to be gasified as soon as it enters the reactor and free C_s is assumed to be present in virgin medical waste. The values of relevant kinetic data and heat of pyrolysis are adopted from [53]. Kinetic rate data is given in Table 6.3. And heat of pyrolysis is taken as -20000 J/kg. Finite reaction rates of gasification are implemented through user-defined source terms for species $C_6H_{10}O_5$,CH_4 and CO, and heat of pyrolysis is implemented as user-defined source of energy equation.

Table 6.3
Functional Groups and Kinetic Rate Constants for Waste Pyrolysis [53].

Functional Group	$A_i(s^-1)$	E_i(J/mole)
CO	2.291e+03	61126
CH_4	6.166e+03	69499

Physical and thermodynamic properties of Cellulosic material depend on temperature and polynomial expressions given in [49] are adopted. Since, waste material gasifies instantly at around 700 K, constant properties values, evaluated at 700 K are used in the simulations (see Table 6.4). For gaseous species, default constant values set in FLUENT's material database are used, except for specific heat (C_p). C_P is assumed to be function of temperature only and default polynomial-expressions set in FLUENT are adopted.

Table 6.4
Properties of Cellulose [49].

Density(kg/m^3)	650
C_p(j/kg-K)	2100
Thermal Conductivity(w/m-K)	0.2
Molecular Weight(kg/kmol)	110

In order to complete the numerical model, boundary conditions must be defined. Boundary Conditions for PTDR-100 configuration 1 and 2 are presented in Table 6.5. Solid waste inlet is modeled as "mass flow inlet", outlet is modeled as "outflow" boundary condition. During normal operation of reactor there is approximately 10 kW of heat loss through walls of the reactor. This heat loss is modeled through "wall" boundary condition for the reactor circumferential wall with specified heat flux. Experimentally it is observed that slag temperature at the bottom of the reactor is usually 1800 K. So reactor bottom is modeled as "wall" with fixed temperature. Reactor top and plasma torch walls are modeled as "adiabatic wall" boundary conditions.

In the case of second configuration, as explained before only 10% of actual mass flow rate is considered through solid waste inlet. Remaining 90% is added as volumetric source terms of waste in the slag region at the bottom. The slag region thickness is assumed to be 100 mm. These approximations are consistent with

Table 6.5
Boundary conditions.

Surface	Boundary Type	Configuration 1	Configuration 2
Waste Inlet	Mass flow inlet	flow rate = 60 kg/hr, T = 300 K	flow rate = 6.0 kg/hr, T = 300 K
Torch Inlet	Mass flow inlet	flow rate = 92.6 kg/hr, T analytical model [1]	flow rate = 0.37 kg/hr, T =2000K
Outlet	Outflow	-	-
Circumferential Wall	Wall	-3485W/m^2	-3485W/m^2
Reactor Bottom	Wall	T=1800K	T=1800K
Slag Region	Fluid	-	0.038 kg/m^3 source of waste
Reactor Top	Wall	zero heat flux	zero heat flux

experimental observations. While for the first configuration, all of mass flow rate is considered through solid waste inlet.

The ultimate analysis of typical medical waste used in PTDR-100 is given in Table 6.6. The functional group composition in the waste is approximated according to ultimate analysis and is shown in Table 6.7. As species Cl,N,S,metals and inorganics have very small concentration, they are neglected and additional moisture is added to make up for them.

Comprehensive modeling of the plasma torch is avoided by appropriate boundary conditions at the plasma torch inlets. For the first configuration of PTDR-100, analytical model developed by Rat and Couder [1] is adopted to calculate air flow velocity and temperature at the torch exit. The velocity and enthalpy profile predicted by this analytical model is shown in Fig.6.3. The details of air plasma properties and

Table 6.6
Ultimate analysis of medical waste.

Component	Concentration (wt%)
C	46.39
H	7.3
Cl	1.6
O	25.88
N	0.568
S	0.19
Moisture	8.4
Metals	1.835
Inorganic	7.836

Table 6.7
Functional Group composition of medical waste.

FG	Concentration (wt%)
CH_4	29.2
CO	45.29
C	4.69
H_2O	20.82

the analytical model are given in Appendix A and B , respectively. For the second configuration, as per experimental observations, cathode inlet is modeled as “mass flow rate” boundary condition with 2000 K temperature and 0.37 kg/hr mass flow rate.

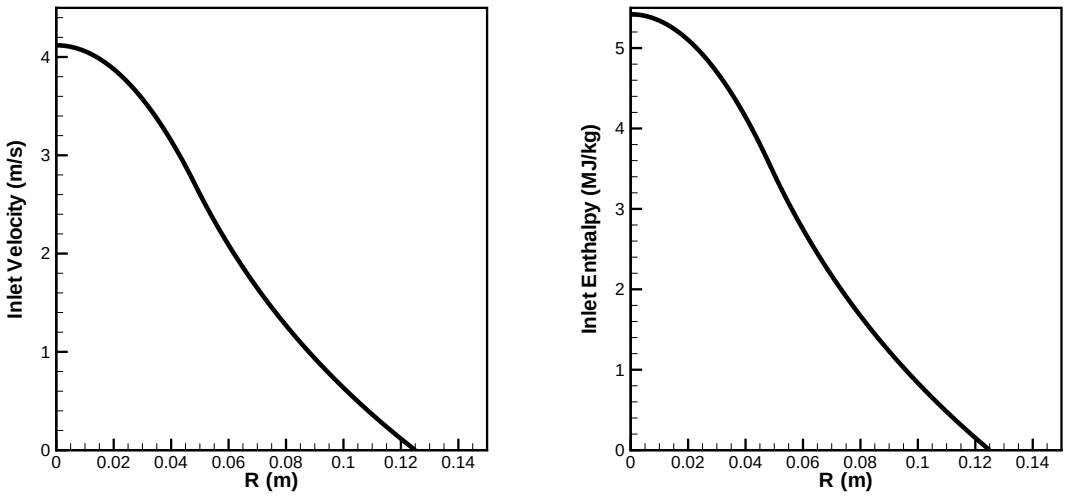

Figure 6.3. Radial profiles of plasma torch inlet velocity (left) and enthalpy (right) derived from the analytical model of Rat and Coudert [1].

7. RESULTS AND DISCUSSIONS

The predictive capabilities of numerical model are demonstrated by comparing four different geometries of the PTDR-100. The reliability of numerical simulations is verified by comparing experimental data obtained from second generation of the PTDR-100. Once it is established that gasification process of medical waste inside the reactor is adequately simulated, the analysis of results is performed by comparing pathlines, residence time distribution, temperature field and species concentration in four different geometries.

The large computing demands imposed the parallel processing using a network of LINUX workstations. In parallel version of FLUENT the grid is partitioned into multiple sub-domains so that number of partitions is an integer multiple of the number of available computing nodes and solver then simultaneously calculates the solution using multiple nodes. For all cases simulated here, the physical convergence criteria is met in maximum of 2500 iterations.

7.1 Validation

The experimental data available for second generation of PTDR-100, with outlet at top, are : bulk temperature of the reactor at bottom and mid section, synthesis gas composition and temperature at the outlet. Fig 7.1 shows the contours of static temperature (K) at plane y=0.0 and outlet surface. Experimentally it is observed that bulk temperature in the lower sections of reactor is around 1300 K and that in the region around solid waste inlet is about 1000 K. From the contour plot it can be noticed that simulated temperatures in these regions are about 1500 K and 1300 K respectively. Overestimation of the temperatures can be attributed to P-1 radiation heat transfer model. As mentioned earlier, P-1 model tends to over-predict

the radiative heat fluxes. Whereas, outlet gas temperature values match very closely, i.e. around 1500K.

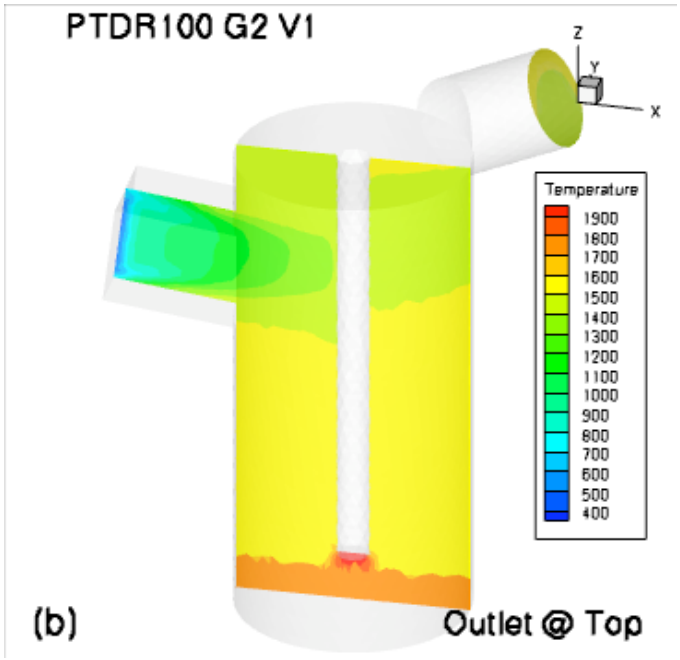

Figure 7.1. Validation with Experimental Data: Static temperature contours (K) at y=0.0 and outlet.

Table 7.1 shows the comparison of experimentally observed and simulated synthesis gas composition at outlet surface. As the main objective of the reactor is to convert medical waste into synthesis gas (CO and H_2), major components of the outlet gas are CO and H_2 species. Numerical model prediction shows that outlet gas mainly consists of CO, H_2 and CH_4. Volume concentrations of CO and H_2 fairly matches with the experimental data. Experimentally no methane (CH_4) gas is observed at the outlet, whereas 17% (by volume) of methane gas is predicted by numerical model. This discrepancy can be attributed to approximations made, while adjusting functional group composition of medical waste. Components like Cl, F, I, S and N found in the ultimate analysis of waste, were neglected for simplifications. These components are part of acid gases and H_2S present in the outlet gas. Due to approximations made, hydrogen (H) present in these gases was accommodated in CH_4 functional

Table 7.1
Comparison of experimental and simulated data.

Synthesis gas composition at reactor outlet	Simulated (%vol)	Experimental (%vol)
CO	41	35.70
H_2	39.38	39
N_2	0.04	22.31
CH_4	17	0
H_2O	0	0
CO_2	2.13	0
C_s (particulates)	0.83	2.11
H_2S	0	0.06
Acid gases (HCl,HF,HI)	0	0.44

group, hence methane is observed in the predicted outlet gas composition of numerical model. Also, as nitrogen, metals and inorganic present in the waste are neglected, very small N_2 and particulate compositions are predicted by simulation, compared with experimental values. Considering the great complexity of physical and chemical processes, such as solid-gas multiphase flow and gasification, taking place in thermal plasma reactor has to be approximated for numerical model development, it can be concluded that numerical model predictions are quite satisfactory, despite some differences.

After validating numerical model with the experimental data and concluding that the process is adequately simulated, the analysis of results concerning pathlines, species concentration, residence times and temperature field is performed for comparison of different geometries of PTDR-100. Contour plots on surface y=0.0 are used for comparison. This plane is chosen, because the region at the waste inlet is visible clearly and variations near waste inlet are important for analysis.

7.2 Geometry Comparison

7.2.1 Performance Evaluation

First, the comparison between two main generations of PTDR-100 is performed. The first generation is characterized by direct interaction of solid waste with the plasma jet and hence, high temperatures and high mass flow rate of plasma forming gas, i.e. air. While in the second generation, plasma assembly is isolated from the main reaction zone by Silicon-Carbide tiles, hence no direct plasma-waste interaction, relatively lower temperatures and very little mass flow rate of air. In Fig. 7.2 temperature contours predicted by numerical model are shown for both the reactors. It is quite evident that temperatures in first generation are considerably higher (>3000K) compared to second generation, where almost uniform temperature of 1500 K is observed. In both the generations, despite chemical reactions, temperature field distribution is almost uniform. This can be attributed to the heat of various gasification and gas phase reactions. Gasification reactions are endothermic and some of gaseous phase reactions, such as formation of CO_2 are exothermic. Hence, energy sink by gasification is compensated by energy source due to gas phase reactions.

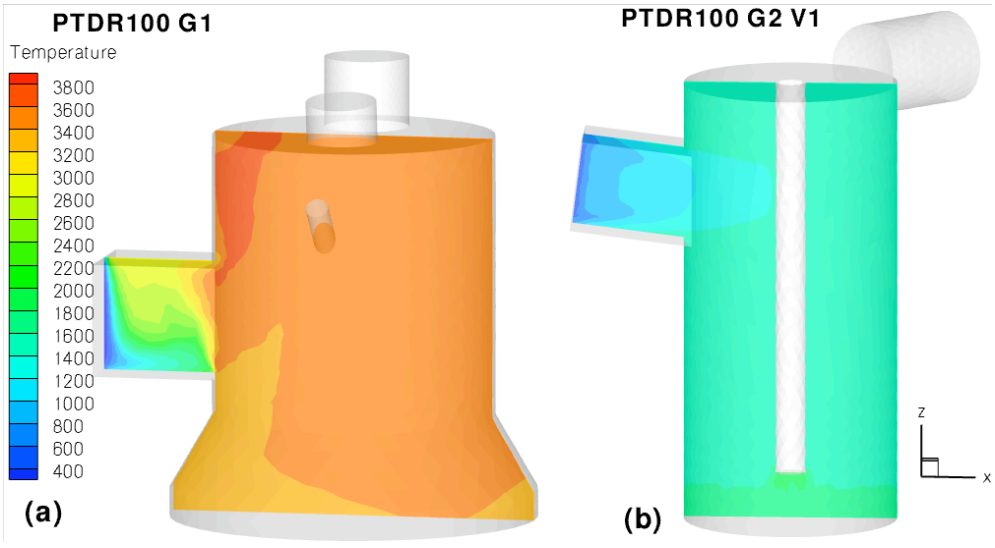

Figure 7.2. Comparison of PTDR-100 generation 1(a) and 2(b): Static temperature (K).

High temperatures and high energy densities generated by plasma are key advantages of thermal plasma reactor in waste-to-energy applications. So it may be guessed that first generation performs better than second generation in terms of converting waste into synthesis gas (CO,H_2). But, that is not the case. It is clear from the comparisons of various species evolution in the reactor, shown in Figures 7.3-7.9. In both the generations, high temperature in the reactor causes waste to instantly gasify as soon as it enters through the waste inlet. This can be observed from the contour plots of waste species in Fig. 7.3. Because of the high mass flow rate of air required by two plasma torches employed in the first generation, the O_2 species mass fraction supplied by air is quite significant compared to the second generation, shown in Fig. 7.4.

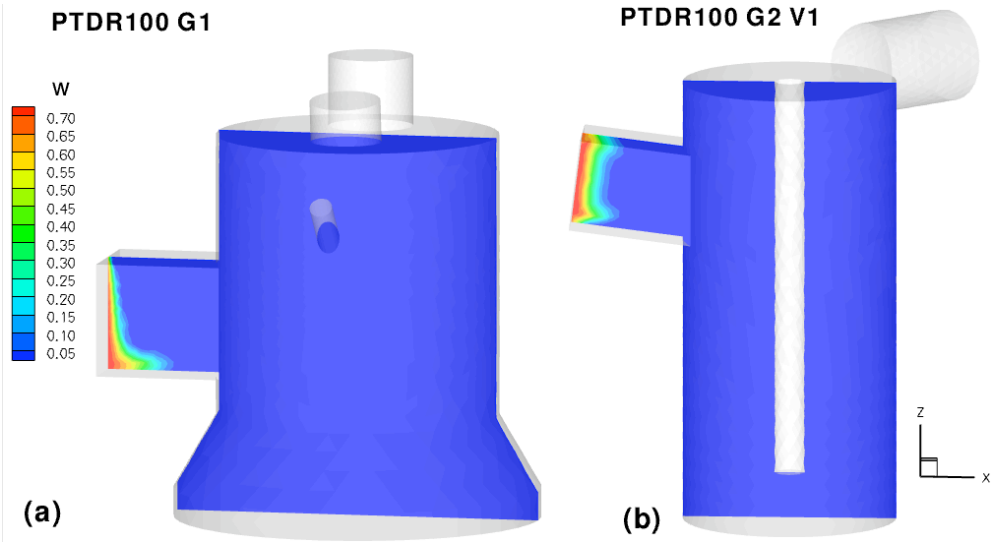

Figure 7.3. Comparison of PTDR-100 generation 1(a) and 2(b): waste mass fraction.

Presence of excessive oxidizer is not very encouraging for gasification reactors. The discouraging effects of excessive oxidizer can be seen from contour plots of CO,H_2,CO_2 and CH_4 in Figures 7.5,7.6 , 7.7 and 7.8, respectively. The oxidation reactions, producing mainly CO_2, dominate any other gasification reactions. As a obvious consequence, major product species in the reactor are CO_2, whereas CO, H_2

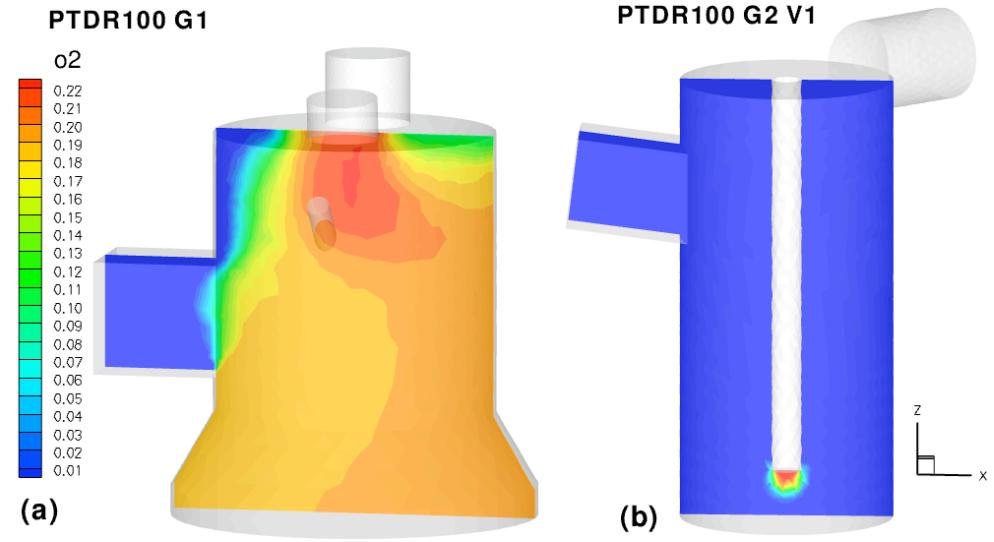

Figure 7.4. Comparison of PTDR-100 generation 1(a) and 2(b): O_2 mass fraction.

and CH_4 are produced in negligibly small amounts. In the second generation, limited amount of O_2 species are present. Almost all of O_2 is consumed at the cathode inlet location. The major species present in the reactor chamber are CO and CH_4. Presence of CO_2 species is also considerable, but significantly less compared to that in the first generation. In the both reactors, as seen from Fig. 7.9, H_2O species are consumed in various steam shift reactions and do not contribute in product gas composition. Based on these observations it is suggested that second generation of PTDR-100 reactor performs more effectively, as a waste gasifier, compared to the first generation.

7.2.2 Effects of outlet location

In the last section, it is observed that generation 2 of PTDR-100 reactor is more effective than generation 1 . CFD model is used to compare effects of three different outlet positions on the mixing and residence time distribution. Sufficient amount of mixing and residence times are important to allow complete gasification of solid waste and conversion of higher hydrocarbons into lighter ones through gas phase reactions.

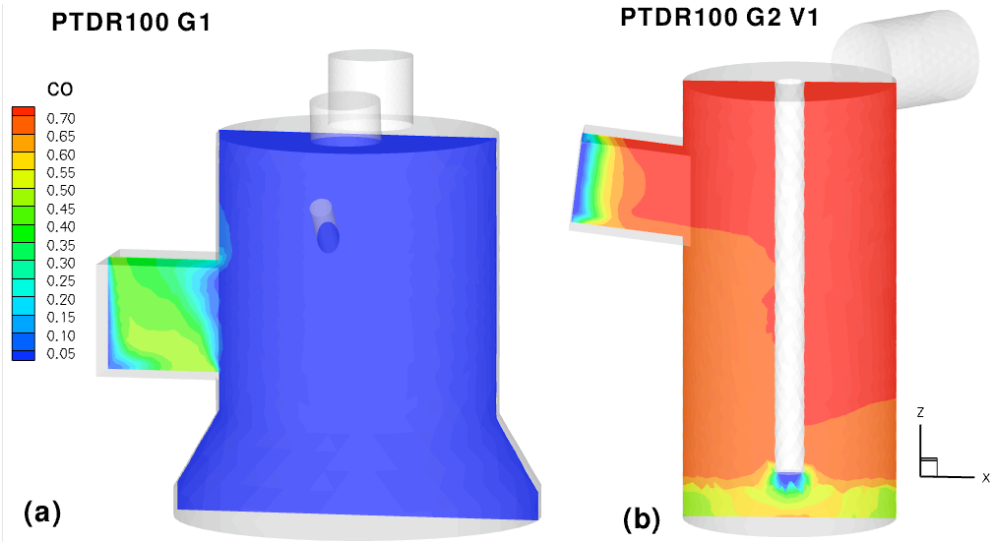

Figure 7.5. Comparison of PTDR-100 generation 1(a) and 2(b): CO mass fraction.

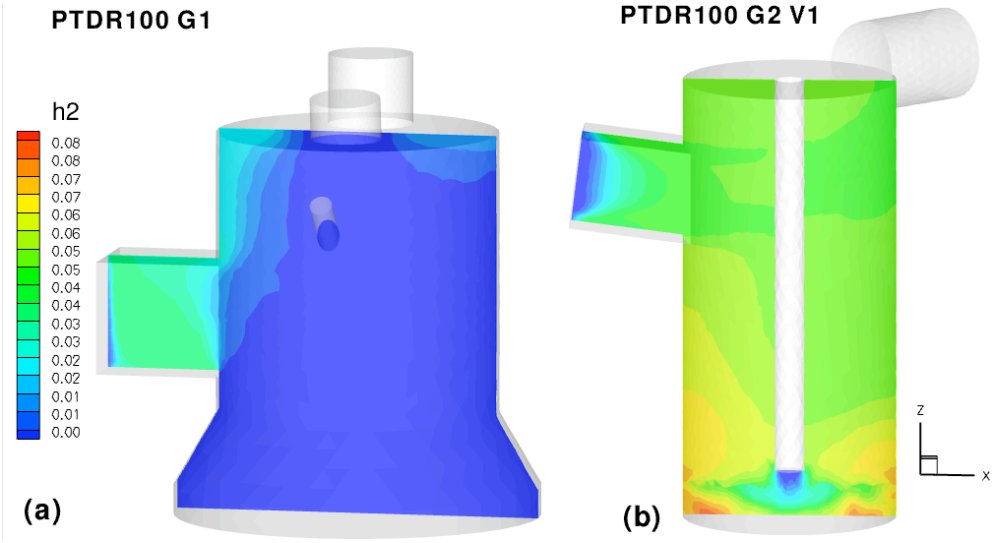

Figure 7.6. Comparison of PTDR-100 generation 1(a) and 2(b): H_2 mass fraction.

Three different axial positions of outlet are considered. In version 1, outlet is located near the the top, in version 2 outlet is 300 mm away from the top and in version 3 it is distanced 500 mm from the top surface.

For analyzing mixing, pathlines from solid inlet, air inlet and bottom region are plotted, as shown in Fig.7.10-7.12. It can be observed that mixing is not significantly

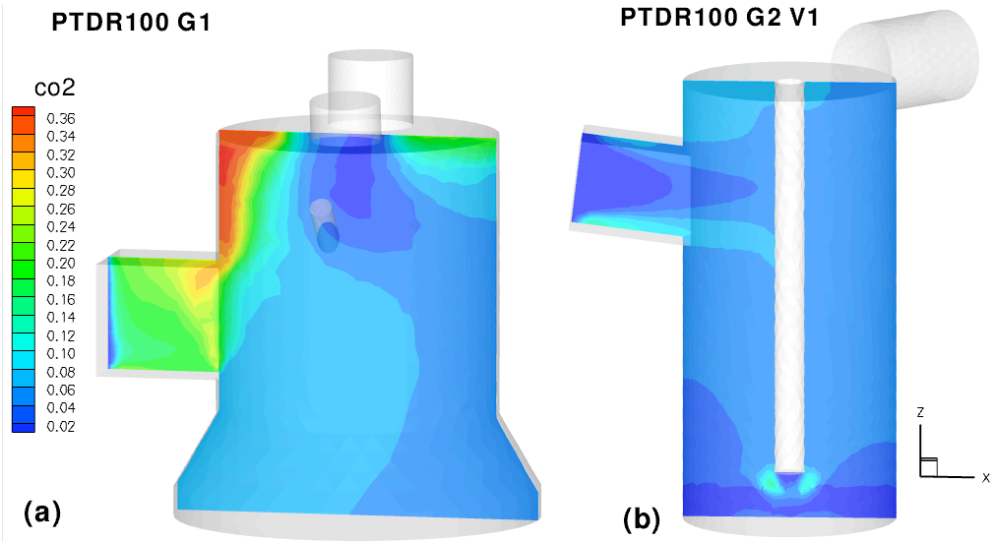

Figure 7.7. Comparison of PTDR-100 generation 1(a) and 2(b): CO_2 mass fraction.

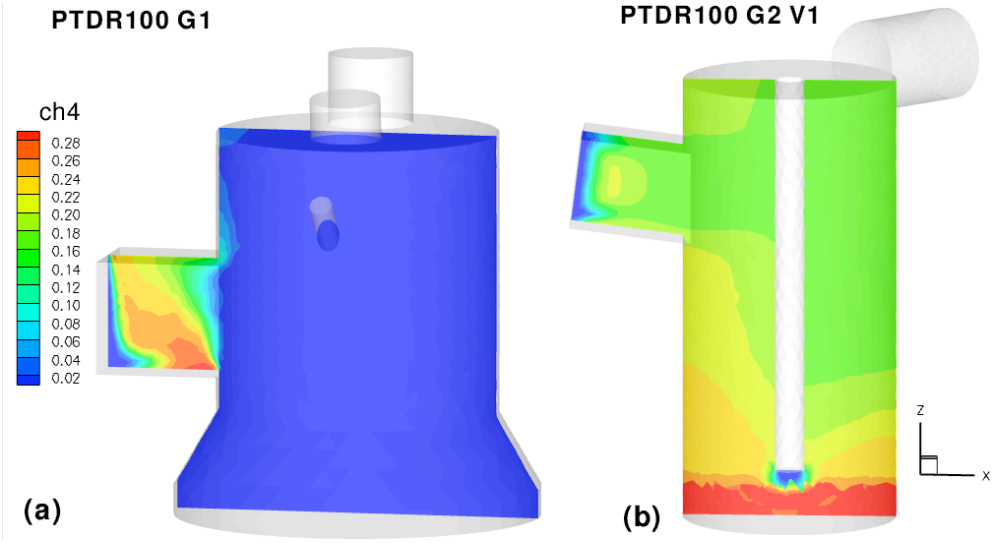

Figure 7.8. Comparison of PTDR-100 generation 1(a) and 2(b): CH_4 mass fraction.

affected by the three different outlet positions. Pathlines show that for all the three locations of outlet, most of the gasification species produced near the waste inlet region, exit reactor without much mixing.

Observations of mixing from the pathlines can be confirmed by plotting residence time distribution for solid waste inlet species. The pulse method is employed

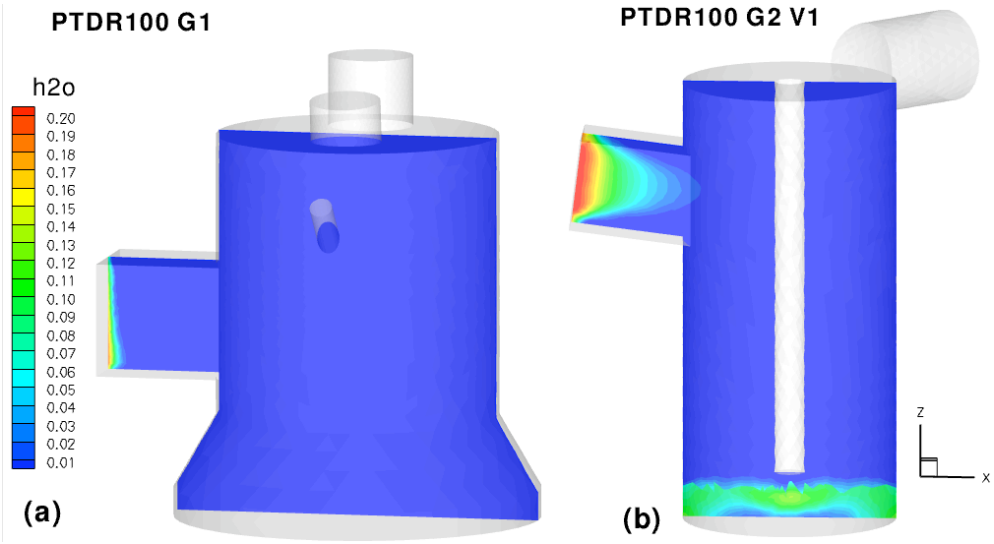

Figure 7.9. Comparison of PTDR-100 generation 1(a) and 2(b): H_2O mass fraction.

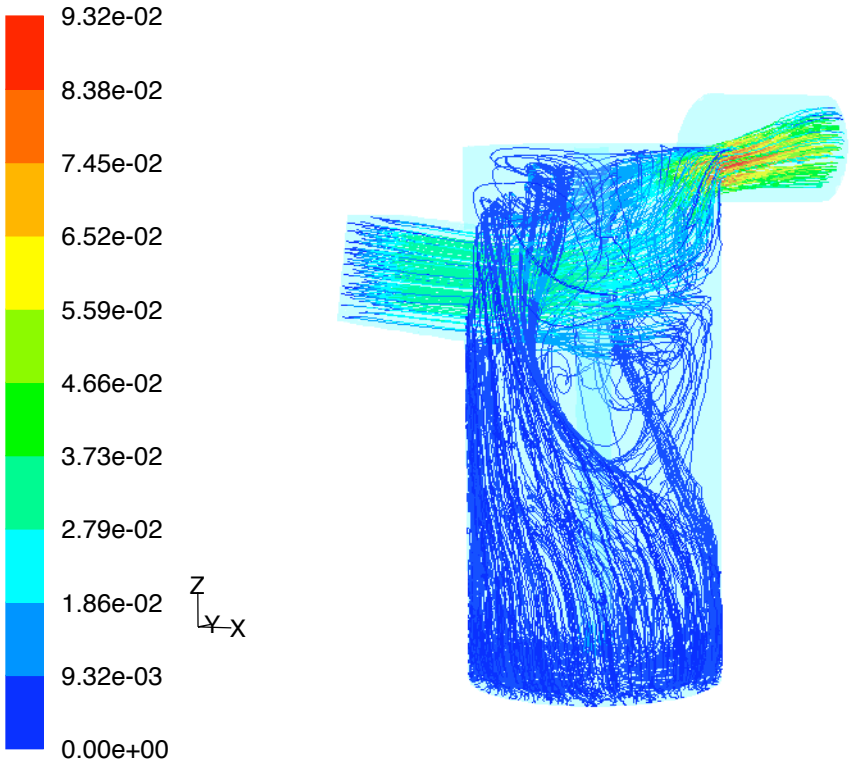

Figure 7.10. Pathlines colored by velocity in PTDR-100 version 1.

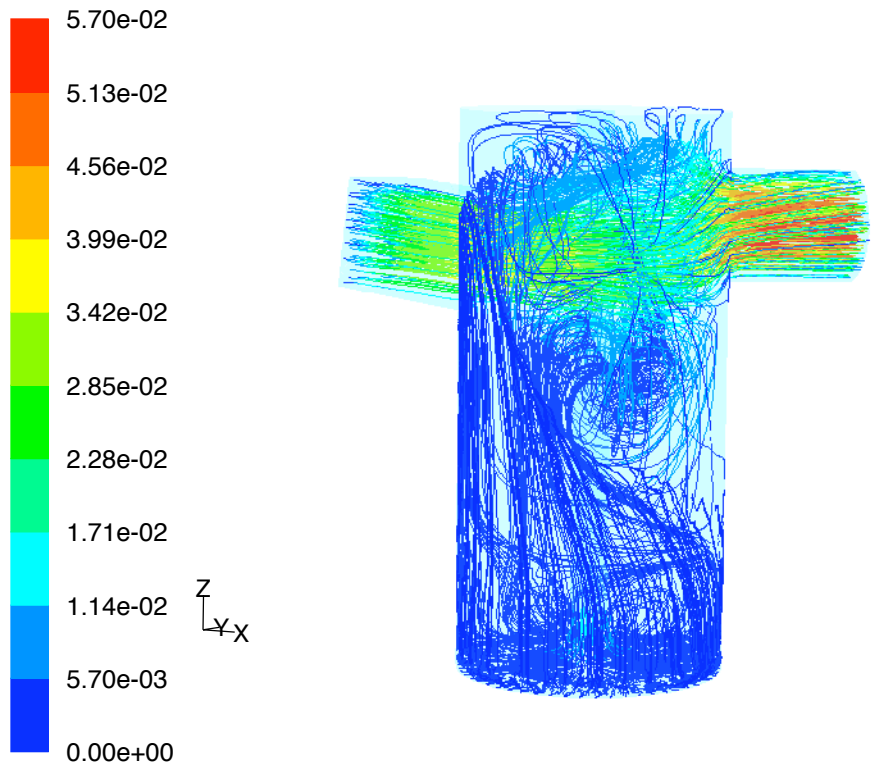

Figure 7.11. Pathlines colored by velocity in PTDR-100 version 2.

to calculate the residence time distribution. In this method, using converged steady state solution as initial data, the tracer is injected from the inlet at time t=0. The tracer species concentration at the inlet is increased to one for the first time step, and then be reset to zero for second and subsequent time steps. A plot of tracer concentration(C) versus time (t) at the outlet provides the residence time distribution. The mean residence time (t_{res})is then calculated as:

$$t_{res} = \frac{\sum_i t_i C_i}{\sum_i C_i} \tag{7.1}$$

Fig. 7.13 shows the comparison of residence time distribution. The mean residence times, calculated using Eq. (7.1), are 95.43 s, 93.03 s and 93.42 s for version 1, 2 and 3 respectively. As referred from pathlines , there is no significant difference

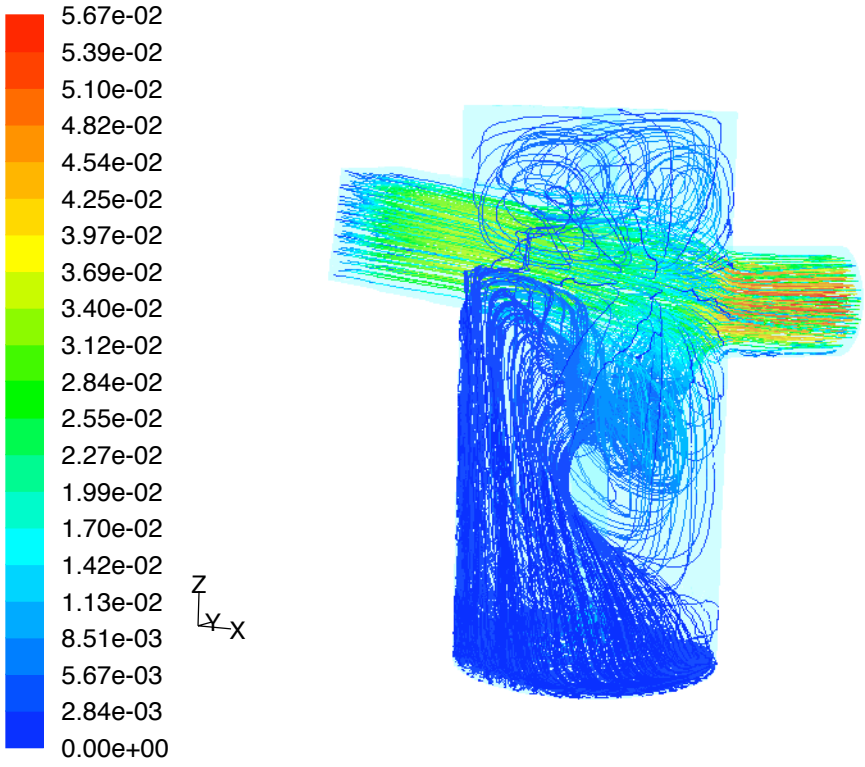

Figure 7.12. Pathlines colored by velocity in PTDR-100 version 3.

between residence time distribution. Hence, it can be concluded that three outlet positions, considered here, do not significantly affect mixing and residence times.

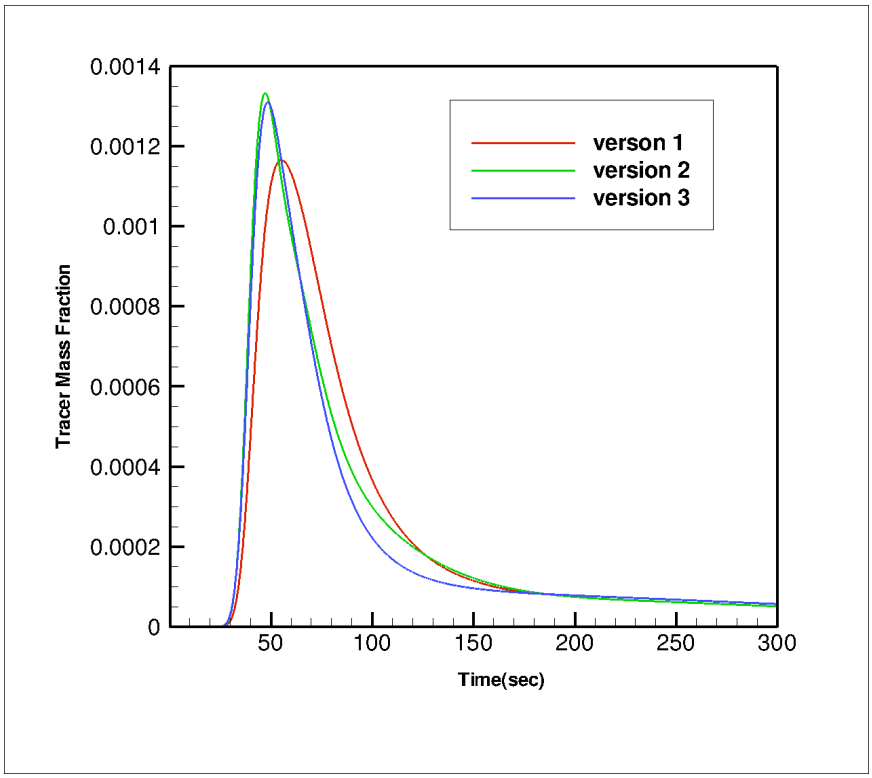

Figure 7.13. Residence time distribution for three different outlet positions of PTDR-100.

8. CONCLUSIONS AND FUTURE WORK

8.1 Conclusions

In this work, thermal plasma application in solid waste treatment has been demonstrated. Thermal plasma technology has a potential for transforming organic waste into energy and non-leachable residue. Various advantages of thermal plasma over conventional waste incineration process are explained. Numerical modeling of transferred arc and non-transferred arc are presented. Pyrolysis and gasification reaction mechanisms and kinetics for various kinds of waste are explained.

The main objective of demonstrating CFD model application in analyzing thermal plasma reactor is achieved. At the moment, available numerical models can not stand up to the multi-dimensional modeling of gasification of solid waste in thermal plasma reactor. Hence, key approximations based on experimental observations need to be made to develop a CFD model of plasma reactor. CFD model presented here is developed in the framework of commercial code FLUENT 6.3 and includes sub-models, such as standard 2-eqn k-ϵ turbulence model, species transport with eddy dissipation for gas phase reactions, P-1 model for radiation heat transfer and functional group approach for solid waste gasification. An industrial thermal plasma reactor PTDR-100 has been analyzed using this CFD model.

As a first step, numerical model is validated against available experimental data. Product gas composition and temperatures at the outlet, predicted by CFD model and experiments are compared. It is observed that CFD model predicts temperature and CO, H_2 species composition at the outlet quite well. Few discrepancies in predicted composition of species like CH_4 and N_2 can be attributed to approximations made in calculating functional group composition of simulated medical waste. Over-prediction of bulk temperatures the inside reactor is because of P-1 radiation model, which may

overestimate the radiation heat fluxes. In general, it is concluded that developed numerical model adequately models the thermal plasma reactor and can be used for further design analysis.

Two different configurations of PTDR-100 are evaluated based on effectiveness of converting solid waste into synthesis gas (CO and H_2). In the first configuration, where solid waste directly interacts with plasma, concentration of O_2 inside reactor is higher than that in the second configuration of PTDR-100. As a result, concentration of synthesis gas species inside the first reactor is smaller than that in the second. Hence, it is concluded that, despite high temperatures in the first reactor , it is less effective in transforming solid waste into synthesis gas compared to the second reactor.

After establishing that second configuration of PTDR-100 is more effective, effects of outlet position on the mixing and residence time distribution are evaluated. Three different outlet positions are considered. For comparing mixing efficiency pathlines are plotted inside the reactor. From the pathlines, it is observed that there is not much difference in mixing characteristics of reactor for three different outlet positions. This observation is confirmed by computing residence time distribution. The mean residence times for all three cases are found to be nearly same. Hence, it is concluded that three outlet positions do not significantly affect reactor mixing characteristic and residence times.

8.2 Future Work

In the current work, the main objective was to check applicability of CFD modeling techniques to simulate various processes involved in plasma pyrolysis. Plasma pyrolysis is a complex phenomena and poses significant challenges for numerical modeling. This being our first attempt, several simplifications and approximations had to be made. The simplified numerical model, developed in this work, demonstrated that CFD can play critical role in design analysis of thermal plasma reactor. After establishing the applicability of CFD modeling, current numerical model can be improved by using more sophisticated physical sub-models and relaxing approximations.

First step in the future work can be directed towards applying more complete reaction kinetics for gasification. In the current model, only four major functional groups (CO,CH_4,H_2,H_2O) are considered. Reaction mechanism model can be improved by considering other functional groups, such as C_2H_4, C_2H_6 etc. Also, as there is large diversity in the values of kinetic data for waste gasification, more sophisticated approach of Distributed Activation Energy (DAEM) can be employed for better accuracy. DAEM approach can be implemented in CFD model as presented by [56].

Although, CFD modeling of plasma jet has been demonstrated, it is not included directly in the numerical model of plasma reactor. Detail plasma modeling can improve the accuracy of waste gasification simulations, especially when solid waste is directly injected into the plasma. In the plasma mathematical model, laminar flow is assumed. But in reality, plasma gas is characterized by magnetohydrodynamic (MHD) turbulence phenomena. Plasma numerical model can be improved, in the future work, by employing appropriate physical sub-model to account for turbulence.

Reacting solid-gas coupled flow is still a challenging problem for numerical analysis. The option of porous media approximation for solid waste can be considered in the future work. An attempt should be made to address the stability issues, when moving porous media is considered. This will present solid flow inside reactor more closely to the actual process and flow field values predicted by this model will be more accurate.

CFD can play important role in analyzing plasma pyrolysis of solid waste. Comprehensive simulation of complex processes involved in plasma pyrolysis is an unreachable target. However, careful approximations derived from experimental observations may help in simulating the process adequately. With constant improvements in current numerical models, sophisticated CFD tool can be developed to represent thermal plasma pyrolysis process more accurately.

LIST OF REFERENCES

LIST OF REFERENCES

[1] V. Rat and J. F. Coudert. A simplified analytical model for dc plasma spray torch: Influence of gas properties and experimental conditions. *Journal of Physics D: Applied Physics*, 39:4799–4807, 2006.

[2] H. Huang and L. Tang. Treatment of organic waste using thermal plasma pyrolysis technology. *Energy Conversion and Management*, 48:1331–1337, 2007.

[3] E. Gomez, D. Amutha Rani, C. R. Cheeseman, D. Deegan, M. Wise, and A. R. Boccaccini. Thermal plasma technology for the treatment of wastes: A critical review. *Journal of Hazardous Materials*, 161:614–626, 2009.

[4] B. V. Babu. Chemical kinetics and dynamics of plasma-assisted pyrolysis of assorted non-nuclear waste. http://discovery.bits-pilani.ac.in/discipline/chemical/BVb.

[5] S. Ravelli, A. Perdichizzi, and G. Barigozzi. Description , applications and numerical modelling of bubbling fluidized bed combustion in waste-to-energy plants. *Progress in Energy and Combustion Science*, 34:224–253, 2008.

[6] Won Yang, Hyung Nam, and Sangmin Choi. Improvements of operating conditions in waste incinerators using engineering tools. *Waste Management*, 27:604–613, 2007.

[7] C. Ryu, Y. B. Yang, V. Nasserzadeh, and J. Swithenbank. Thermal reaction modelling of a large municipal solid waste incinerator. *Combustion Science and Technology*, 176:1891–1907, 2004.

[8] C. Ryu and S. Choi. 3-dimensional simulation of air mixing in the MSW incinerators. *Combustion Science and Technology*, 119:155–170, 1996.

[9] C. Ryu, D. Shin, and S. Choi. Combined simulation of combustion and gas flow in a grate-type incinerator. *Journal of Air and Waste Management Association*, 52:189–197, 2002.

[10] M. Miltner, A. Makaruk, M. Harasek, and A. Fiedl. Computational fluid dynamic simulation of a solid biomass combustor: modelling approaches. *Clean Technologies and Environmental Policy*, 10(2):165–174, 2008.

[11] C. D. Goddard, Y. B. Yang, J. Goodfellow, V. N. Sharifi, J. Swithenbank, J. Chartier, D. Mouquet, R. Kirkman, D. Barlow, and S. Moseley. Optimisation study of a large waste-to-energy plant using computational modelling and experimental measurements. *Journal of Energy Institute*, 78(3):106–116, 2005.

[12] MMaher I. Boulos, Pierre Fauchais, and Emil Pfender. *Thermal Plasmas - Fundamentals and Applications*, volume 1. Plenum Press, New York, 1994.

[13] E. Pfender. Thermal plasma technology: Where do we stand and where are we going? *Plasma Chemistry and Plasma Processing*, 19(1), 1999.

[14] S. K. Nema and K. S. Ganeshprasad. Plasma pyrolysis of medical waste. *Current Science*, 83(3):271–278, 2002.

[15] R. R. Guddeti, R. Knight, and E. D. Grossmann. Depolymerization of polyethylene using induction-coupled plasma technology. *Plasma Chemistry and Plasma Processing*, 20(1):37–64, 2000.

[16] Pierre Fauchais and Armelle Vardelle. Thermal plasmas. *IEEE Transactions on Plasma Science*, 25(6), 1997.

[17] Seungho Paik and Hoa D. Nguyen. Numerical modeling of multiphase plasma/soil flow and heat transfer in an electric arc furnace. *International Journal of Heat and Mass Transfer*, 38(7):1161–1171, 1995.

[18] J. J. Gonzalez, P. Freton, and A. Gleizes. Theoretical study of hydrodynamic flow in thermal plasma devices. *Czechoslovak Journal of Physics*, 56:B721–B732, 2006.

[19] J. F. Bisson, B. Gauthier, and C. Moreau. Effect of plasma fluctuations on in-flight particle parameters. *Journal of Thermal Plasma Spray Technology*, 12(1):38–43, 2003.

[20] P. Eichert, M. Imbert, and C. Coddet. Numerical study of an ArH_2 gas mixture flowing inside and outside a dc plasma torch. *Journal of Thermal Spray Technology*, 7(4):505–512, 1998.

[21] Peng Han and Xi Chen. Modeling of the subsonic-supersonic flow and heat transfer in a dc arc plasma torch. *Plasma Chemistry and Plasma Processing*, 21(2), 2001.

[22] X. Q. Yuan, H. Li, T. Z. Zhao, W. K. Guo, and P. Xu. Effects of nozzle configuration on flow characteristics inside dc plasma torch. *Japanese Journal of Applied Physics*, 43(10):7249–7253, 2004.

[23] Min Hur, Tae Hyung Hwang, Won Tae Ju, Chan Min Lee, and Sang Hee Hong. Numerical analysis and experiments on transferred plasma torches for finding appropriate operating conditions and electrode configuration for a waste melting process. *Thin Solid Films*, 390:186–191, 2001.

[24] S. W. Chau, K. L. Hsu, D. L. Lin, J. S. Chen, and C. C. Tzeng. Modeling and experimental validation of a 1.2 MW dc transferred well-type plasma torch. *Computer Physics Communications*, 177:114–117, 2007.

[25] Pierre Freton, Jean-Jacques Gonzalez, Alain Gleizes, Gaelle Escallier, and Bruno Van Ootegem. Arc movements in a hollow cathode of a high-power plasma torch. *IEEE Transactions of Plasma Science*, 36(4):1044–1045, 2008.

[26] J. H. Seo, J. M. Park, and S. H. Hong. Influence of dc arc jets on flow fields analyzed by an integrated numerical model for a dc-rf hybrid plasma. *Plasma Sources Science and Technology*, 17, 2008.

[27] Frank Karetta and Manfred Lindmayer. Simulation of the gasdynamic and electromagnetic processes in low voltage switching arcs. *IEEE Transactions on Components, Packaging, And Manufacturing Technology*, 21(1):96–103, 1998.

[28] J. Menart, S. Malik, and L. Lin. Coupled radiative, flow and temperature-field analysis of a free-burning arc. *Journal of Physics D: Applied Physics*, 33:257–269, 2000.

[29] V. Aubrecht and B. Gross. Net emission coefficient of radiation in SF_6 arc plasmas. *Journal of Physics D: Applied Physics*, 27:95–100, 1994.

[30] A. Essoltani, P. Proulx, and M. I. Boulos. Radiation and self-absorption in argon-iron plasmas at atmospheric pressure. *Journal of Analytical Atomic Spectrometry*, 5:543–547, 1990.

[31] J. Menart and S. Malik. Net emission coefficients for argon-iron thermal plasmas. *Journal of Physics D: Applied Physics*, 35:867–874, 2002.

[32] Y. Naghizadeh-Kashani, Y. Cressault, and A. Gleizes. Net emission coefficient of air thermal plasmas. *Journal of Physics D: Applied Physics*, 35:2925–2934, 2002.

[33] Pavel Kotalík. Modelling of an argon plasma flow. *Czechoslovak Journal of Physics*, 55(2):173–188, 2005.

[34] S. D. Eby, J. Y. Trépanier, and X. D. Zhang. Modelling radiative transfer in SF_6 circuit-breaker arcs with the p-1 approximation. *Journal of Physics D: Applied Physics*, 31:1578–1588, 1998.

[35] Z. Sun, M. Rong, Y. Wu, J. Li, and F. Yang. Three-dimensional numerical analysis with P-1 radiation model in low voltage switching arc. *IEICE Transactions on Electronics*, E90-C(7):1348–1355, 2007.

[36] D. Bernardi, V. Colombo, E. Ghedini, and A. Mentrelli. Comparison of different techniques for the FLUENT-based treatment of the electromagnetic field in inductively coupled plasma torches. *The European Physics Journal D*, 27:55–72, 2003.

[37] Ayhan Demirbaş. Biomass resource facilities and biomass conversion processing for fuels and chemicals. *Energy Conversion and Management*, 42:1357–1378, 2001.

[38] G. Tchobanoglous, H. Theisen, and S. Vigil. *Integrated Solid Waste Management : Engineering Principles and Management Issues*. McGraw-Hill, Inc., 1993.

[39] Ayhan Demirbaş. An overview of biomass pyrolysis. *Energy Sources*, 24:471–482, 2002.

[40] Dough Orr and David Maxwell. A comparison of gasification and incineration of hazardous wastes. *Report by Radiant International LLC for U.S. DOE*, (DCN 99.803931.02), March 30,2000.

[41] A. Mountouris, E. Voutsas, and D. Tassios. Solid waste plasma gasification: Equilibrium model development and exergy analysis. *Energy Conversion and Management*, 47:1723–1737, 2006.

[42] R. A. Kalinenko, A. P. Kuznetsov, A. A. Levitsky, V. E. Messerle, Y. A. Mirokhin, L. S. Polak, Z. B. Sakipov, and A. B. Ustimenko. Pulverized coal plasma gasification. *Plasma Chemistry and Plasma Processing*, 13:141–167, March 1993.

[43] I. B. Georgiev and B. I. Mihailov. Some general conclusions from the results of studies on solid fuel steam plasma gasification. *Fuel*, 71:895–901, August 1992.

[44] D. Djebabra, O. Dessaux, and P. Goudmand. Coal-gasification b microwave plasma in water-vapor. *Fuel*, 70:1473–1475, December 1991.

[45] Lan Tang, H. Huang, Zengli Zhao, C. Z. Wu, and Y. Chen. Pyrolysis of polypropylene in a nitrogen plasma reactor. *Industrial and Engineering Chemistry Research*, 42:1145–1150, 2003.

[46] K. Moustakas, D. Fatta, S. Malamis, K. Haralambous, and M. Loizidou. Demonstration plasma gasification/vitrification system for effective hazardous waste treatment. *Journal of Hazardous Materials*, B123:120–126, 2005.

[47] A. Mountouris, E. Voutsas, and D. Tassios. Plasma gasification of sewage sludge: process development and energy optimization. *Energy Conversion and Management*, (doi:10.1016/j.enconman.2008.01.025), 2008.

[48] Huang Jianjun, Guo Wenkang, and Xu Ping. Thermodynamic study of water-steam plasma pyrolysis of medical waste for recovery of co and h_2. *Plasma Science and Technology*, 7(6), 2005.

[49] B. V. Babu and A. S. Chaurasia. Pyrolysis of biomass: improved models for simultaneous kinetics and transport of heat, mass and momentum. *Energy Conversion and Management*, 45:1297–1327, 2004.

[50] K. Papadikis, H. Gerhauser, A. V. Bridgwater, and S. Gu. Cfd modelling of fast pyrolysis of an in-flight cellulosic particle subjected to convective heat transfer. *Biomass and Bioenergy*, 33:97–107, 2009.

[51] U. Sand, J. Sandberg, J. Larfeldt, and R. Bel Fdhila. Numerical prediction of the transport and pyrolysis in the interior and surrounding of dry and wet wood log. *Applied Energy*, 85:1208–1224, 2008.

[52] Stephen R. Turns. *An Introduction to Combustion: Concepts and Applications*. McGraw Hill, second edition, 2000.

[53] A. Elfasakhany, T. Klason, and X. S. Bai. Modelling of pulverised wood combustion using a functional group model. *Combustion Theory and Modelling*, 12(5):883–904, 2008.

[54] H. M. Zhu, J. H. Yan, X. G. Jiang, Y. E. Lai, and K. F. Cen. Study on pyrolysis of typical medical waste materials by using tg-ftir analysis. *Journal of Hazardous Materials*, 153:670–676, 2008.

[55] J. H. Yan, H. M. Zhu, X. G. Jiang, Y. Chi, and K. F. Cen. Analysis of volatile species kinetics during typical medical waste materials pyrolysis using a distributed activation energy model. *Journal of Hazardous Materials*, 162:646–651, 2009.

[56] A. A. Rostami, M. R. Hajaligol, and S. E. Wrenn. A biomass pyrolysis sub-model for cfd applications. *Fuel*, 83:1519–1525, 2004.

[57] Fluent Inc. Fluent 6.3 documentation, 2006.

[58] R.I. Backreedy, L. M. Fletcher, J. M. Jones, L. Ma, M. Pourkashanian, and A. Williams. Co-firing pulverised coal and biomass: a modeling approach. *Proceedings of the Combustion Institute*, 30:2955–2964, 2005.

[59] J. Fiedler, E. Lietz, D. Bendix, and D. Hebecker. Experimental and numerical investigations of a plasma reactor for the thermal destruction of medical waste using a model substance. *Journal of Physics D: Applied Physics*, 37:1031–1040, 2004.

[60] A. D'Angola, G. Colonna, C. Gorse, and M. Capitelli. Thermodynamic and transport properties in equilibrium air plasmas in a wide pressure and temperature range. *The European Physical Journal D*, 46:129–150, 2008.

[61] P. Freton, J. J. Gonzalez, and A. Gleizes. Comparison between a two- and a three-dimensional arc plasma configuration. *Journal of Physics D: Applied Physics*, 33:2442–2452, 2000.

APPENDICES

APPENDIX A. AIR PLASMA THERMAL AND TRANSPORT PROPERTIES

D'Angola et al. [60] have presented analytical expressions for thermodynamic properties and transport coefficients of air plasmas in a wide pressure (0.01 - 100 atm) and temperature range (50 - 60000 K), ready to be inserted in fluid dynamic codes. The assumption of local thermodynamic equilibrium has been made to describe the plasma with two independent state variables, pressure and temperature.

Polynomial expressions presented by [60] to find air plasma properties like density, specific heat, viscosity, electric conductivity and thermal conductivity as a function of temperature and pressure have been implemented in computer code. Following plots show how these properties vary with temperature at 1 atm pressure.

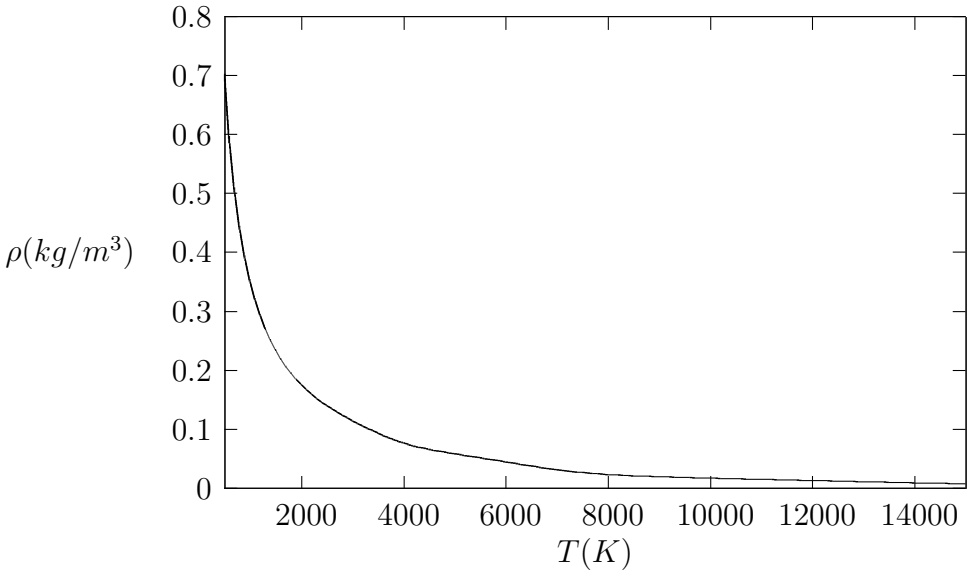

Figure A.1. Density of air plasma as a function of $T(K)$ at 1 atm p.

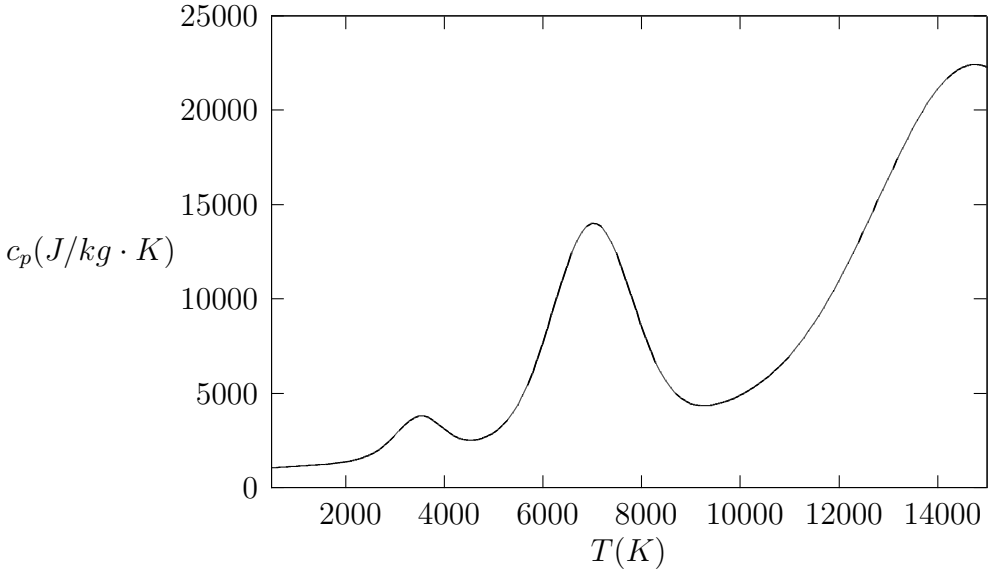

Figure A.2. Specific heat of air plasma as a function of $T(K)$ at 1 atm p.

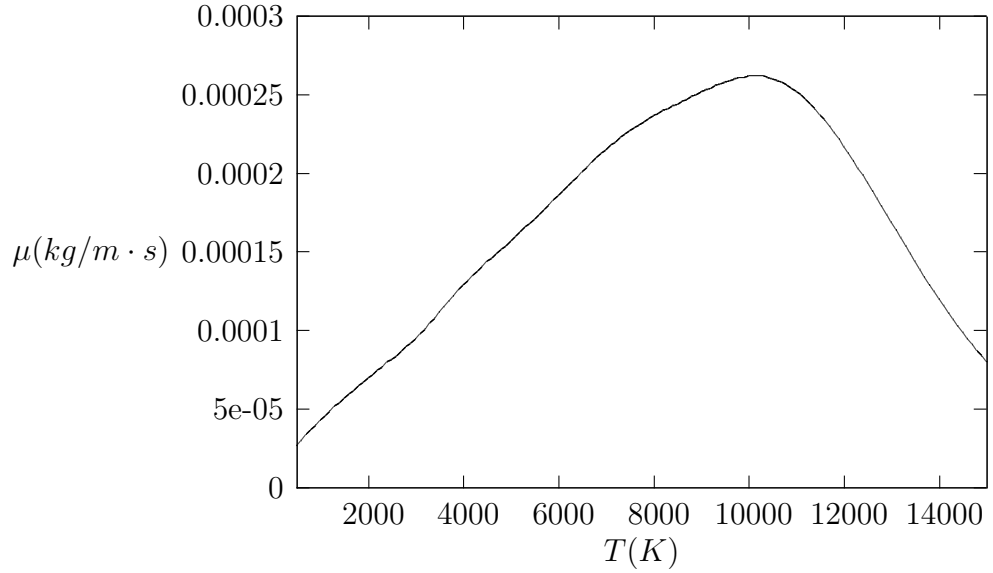

Figure A.3. Viscosity of air plasma as a function of $T(K)$ at 1 atm p.

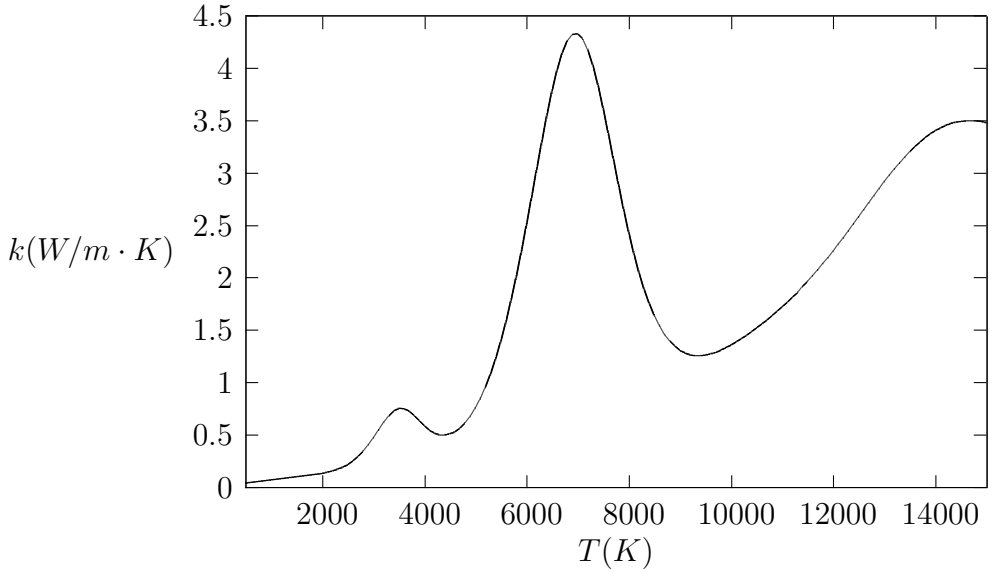

Figure A.4. Thermal conductivity of air plasma as a function of $T(K)$ at 1 atm p.

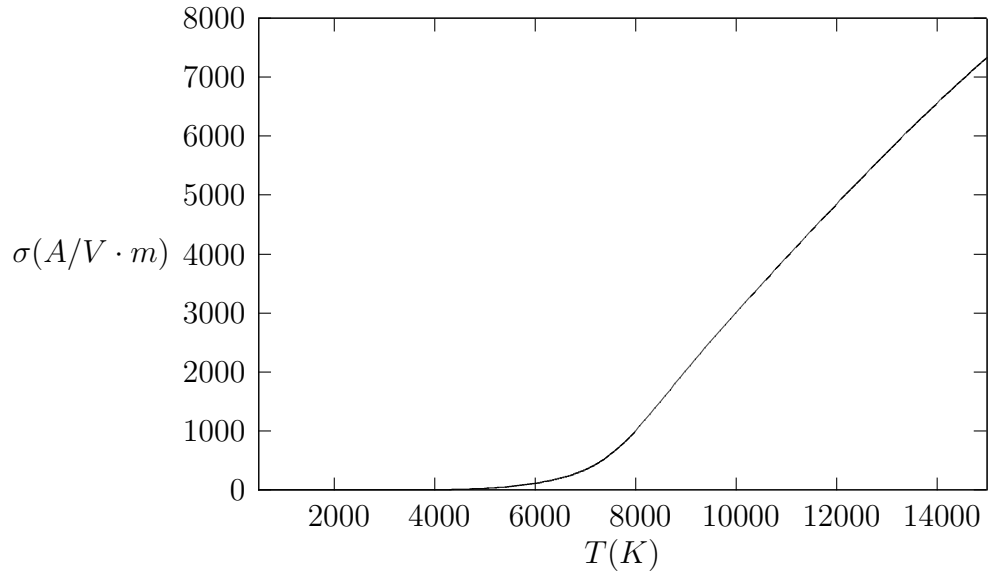

Figure A.5. Electrical conductivity of air plasma as a function of $T(K)$ at 1 atm p.

APPENDIX B. NON-TRANSFERRED ARC MATHEMATICAL MODEL

Alternative approach to complete CFD modeling of the plasma torch is to use analytical model to represent the nozzle exit characteristics of plasma torch as boundary conditions for plasma thermal reactor model. Rat and Coudert [1] present a simplified analytical model for dc plasma torch, in the restricted area of atmospheric plasma spraying conditions. This analytical model derives dc plasma torch properties at nozzle exit using the experimental data, such as specific enthalpy, mean voltage, thermal losses, arc current, nozzle diameter and thermophysical properties of plasma gas. Authors use specific enthalpy to represent thermophysical properties of plasma gases.

It is observed that specific enthalpy varies much faster than temperature, when dissociatoion and ionization takes place. Also dependence of electrical conductivity on specific enthalpy is much more distinguished than on the temperature, where an electrical conduction threshold is defined by critical value of specific enthalpy (h_c), depending on plasma gas. Heat conduction is described in terms of heat potential instead of thermal conductivity, which is found to be linearly dependent on specific enthalpy. Assumption of isentropic plasma flow requires to introduce an averaged isentropic exponent, which is determined by analysing the contributions of pressure acting within the plasma jet. Unsteady characteristics of plasma due to the motion of the arc in the nozzle channel have been neglected by defining time averaged quantities. Also the real plasma flow is assumed to be the same as an insentropic plasma flow which would be generated from reservoir.

B.1 Specific Enthalpy Profile

An analytical expression for the radial profile of specific enthalpy at nozzle exit is derived as a function of easily measured experimental parameters and thermophysical

properties of plasma. The plasma jet is divided into two layers: (1) electrically conducting layer for $h \geq h_c$ and (2) a cold layer (CL) for $h < h_c$. The level of specific enthalpy is determined by electic power input, dissipated by Joule heating, and thermal losses due to radiation escaping from the plasma and heat flow. Hence, the radial profile of specific enthalpy at nozzle exit is give by

$$h = h_c + \Delta h(1 - (r/r_e)^2) \text{ for } 0 \leq r \leq r_e, \tag{B.1}$$

$$h = h_c - \Delta h(\ln(r/r_e) \text{ for } r_e \leq r \leq R \tag{B.2}$$

where r_e is a mean radius, so that $h(r_e) = h_c$, R is radius of torch and Δh is given by

$$\Delta h = |S_h| \cdot r_e^2/4a$$

where S_h is the source term in the energy equation that accounts for effects of Joule heating and radiative losses and a is the linear coefficient that relates the heat potential to the specific enthalpy.

In addition to the approximations stated in the last section, above expression for specific enthalpy is subjected to following assumptions:

- The flow is mainly axial.
- Kinetic energy of the flow is neglected.
- Density of mass flux is constant.
- The interaction between the plasma jet and the external environment is neglected.
- Radial component of heat flow is much higher than the axial one.
- In cold layer (CL) radiative losses and convection of specific enthalpy are neglected.

Δh and r_e are two unknowns, which can be determined by overall thermal balance and condition that $h(R) = 0$. If it is supposed that electrical power supplied to the

torch is converted into the enthalpy flux after removing the heat losses, we get an equivalent specific enthalpy $\bar{h}$ as

$$\bar{h} = \frac{UI - P_{th}}{\dot{m}}, \tag{B.3}$$

where U, I, and P_{th} are mean values of the arc voltage, arc current and torch thermal losses, respectively.

$\bar{h}$ is equivalent to the average specific enthalpy over the nozzle exit cross section:

$$\bar{h} = \frac{2}{R^2} \int_0^R rh(r)\, dr, \tag{B.4}$$

Solving above expression using raial specific enthalpy expressions we get following relation

$$x \ln(y) = \frac{1}{2}y - 1, \tag{B.5}$$

where x and y are

This equation can be solved using Newton-Raphson method along with condition $h(R) = 0$, to give

$$\Delta h = -\frac{h_c}{ln(y)}, \tag{B.6}$$

$$r_e = R\sqrt{y}, \tag{B.7}$$

So using Eq. (B.1), (B.2),(B.6) and (B.7) the radial enthalpy profile is fully determined. This model is then used to determine the plasma axial velocity at the nozzle exit.

B.2 Velocity Profile

Radial enthalpy profile evaluated in the previous section can be assumed to be the stagnation enthalpy along a streamline. Using the Barre de Saint-Venant relationship for an isentropic flow the energy convservation is applied along a streamline crossing the nozzle exit, which yields the formula for plasma axial velocity at nozzle exit:

$$u(r) = v^* \left(\sqrt{1 + \frac{2h(r)}{v^{*2}}} - 1 \right), \tag{B.8}$$

where

$$v^* = \frac{\gamma}{\gamma - 1} \frac{P_a S}{\dot{m}}$$

where γ is the isentropic exponent determined from experiments for various plasma gases, P_a the pressure at the nozzle exit, S is the nozzle cross-section area and $\dot{m}$ is the mass flow rate.

APPENDIX C. TRANSFERRED ARC MATHEMATICAL MODEL

Freton et al. [61] present computational model to compare a two- and a three-dimensional arc plasma configuration, using the commercial code Fluent. They studied two arc plasma configurations: a free burning arc and a transferred arc. In free burning arc, fluid flow is generated only by action of Lorentz forces while in a transferred arc case an inlet mass flow rate is imposed.

C.1 Governing Equations

In plasma, electrically conductive fluid interacts with electromagnetic field. The fluid flow is affected in two ways: (1) application of Lorentz forces as the result of electric current and magnetic field interaction, (2) Joule heating because of electrical resistance.

In the case of plasma generated by applying electric potential across electrodes, the governing equations for electric potential V and potential vector A in 2D axisymmetric configuration can be written as in [61]

$$\frac{\partial}{\partial z}\left(\sigma\frac{\partial V}{\partial z}\right)+\frac{1}{r}\frac{\partial}{\partial r}\left(r\sigma\frac{\partial V}{\partial r}\right)=0 \tag{C.1}$$

$$\frac{\partial^2 A_z}{\partial z^2}+\frac{1}{r}\frac{\partial}{\partial r}\left(r\frac{\partial A_z}{\partial r}\right)+\mu\cdot \jmath_z=0 \tag{C.2}$$

$$\frac{\partial^2 A_r}{\partial z^2}+\frac{1}{r}\frac{\partial}{\partial r}\left(r\frac{\partial A_r}{\partial r}\right)+\mu\cdot \jmath_r-\frac{A_r}{r^2}=0 \tag{C.3}$$

where, V is electric potential, σ is electric conductivity, μ is magnetic permeability, A_z and A_r are radial and axial potential vector components, $\jmath_z$ and $\jmath_r$ are current density components. $\jmath_z$ and $\jmath_r$ components are deduced from the potential:

$$\jmath_z=-\sigma\frac{\partial V}{\partial z} \tag{C.4}$$

$$\jmath_r = -\sigma \frac{\partial V}{\partial r} \tag{C.5}$$

In the above governing equations following assumptions are made [61]:

- Plasma satisfies local thermodynamic equilibrium in steady state.
- The 2D model uses a cylindrical symmetry.
- The gravity effect is neglected.
- Flow is laminar.
- Arc anode interaction is not taken into account.
- Convective terms are set to zero.

The Lorentz force components F_z and F_r acting on the flow field due to electromagnetic coupling are given by:

$$F_z = \jmath_r B_v \tag{C.6}$$

$$F_r = -\jmath_z B_v \tag{C.7}$$

where B_v is azimuthal component of magnetic field, given by the relation

$$B_v = \frac{\partial A_r}{\partial z} - \frac{\partial A_z}{\partial r} \tag{C.8}$$

The energy source E_{joule} due to joule heating is given by

$$E_{joule} = \frac{\jmath_z^2 + \jmath_r^2}{\sigma} \tag{C.9}$$

C.2 CFD Model

The commercial CFD code FLUENT solves Navier-Stokes equations for fluid flow by control volume methods [57]. It has provision of using User Defined Functions (UDF), which are 'user-defined subroutines' required to perform additional computations not available in FLUENT. *UDF* are handy to solve multi-physics fluid flow, like arc plasmas.

UDFs are developed to solve the extra transport equations of electromagnetism and to include source terms in the momentum and energy equations of Navier-Stokes.

C.3 Validation

The free burning plasma arc in 2D axisymmetric configuration, discussed in [61], has been simulated to validate our FLUENT model. C.3.0.1. Definition

Figure C.1 shows the geometry of 2D free burning plasma arc. There is no fluid flow through cathode *AA'* and flow is only generated by the Lorentz forces. The angle of cathode cone is equal to 60^0. The length *BB'* is equal to 4.5 mm. This is to restrict arc attachment to the region along this line. An argon plasma gas at atmospheric pressure operated in an argon environment is considered. C.3.0.2. Boundary Conditions

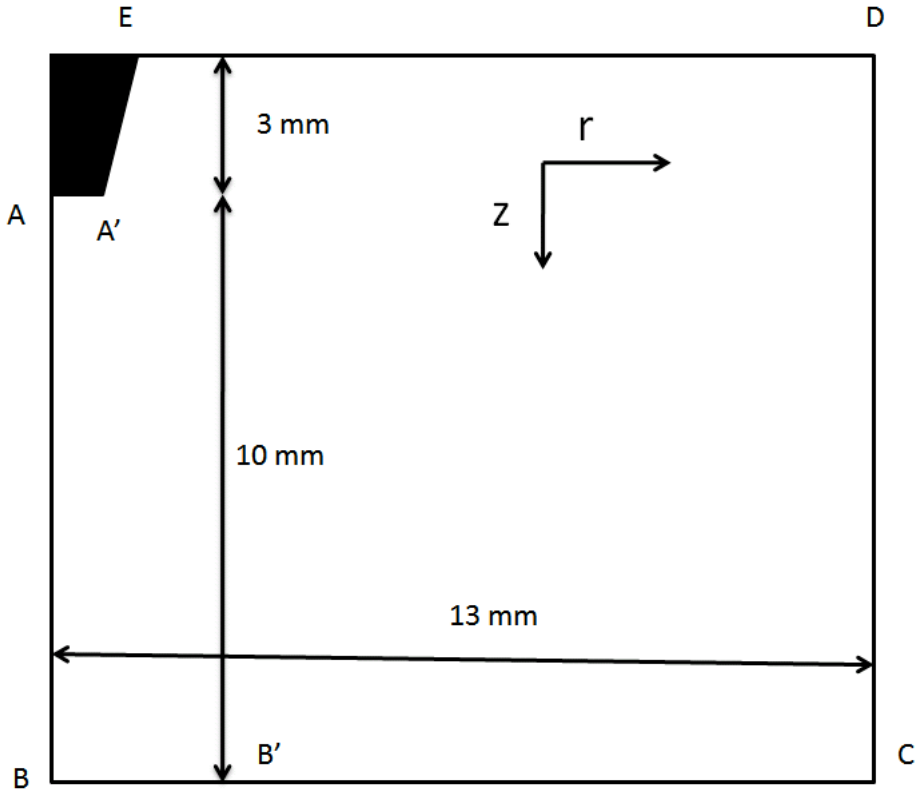

Figure C.1. 2D free burning arc geometry.

The boundary conditions for 2D free burning plasma arc are shown in Table C.1. The potential boundary condition on the line AA' is given by current density distribution j_z:

$$\jmath_z(r) = J_{max} exp(-br) \tag{C.10}$$

where $J_{max} = 1.4 \times 10^8 Am^{-2}$, and $b = 2082.4335$ is determined by

$$I = 2\pi \int_0^{R_c} r\jmath_z(r)\, dr \tag{C.11}$$

with $R_c = 3$ mm.

Table C.1
2D free burning arc boundary conditions.

Boundary	P	u_z	u_r	T	V	A_z	A_r
AB	$\frac{\partial p}{\partial r} = 0$	$\frac{\partial u_z}{\partial r} = 0$	0	$\frac{\partial T}{\partial r} = 0$	$\frac{\partial V}{\partial r} = 0$	$\frac{\partial A_z}{\partial r} = 0$	$\frac{\partial A_r}{\partial r} = 0$
BB'	–	0	0	$\frac{\partial T}{\partial z} = 0$	0	$\frac{\partial A_z}{\partial z} = 0$	$\frac{\partial A_r}{\partial z} = 0$
$B'C$	–	0	0	1000	0	$\frac{\partial A_z}{\partial z} = 0$	$\frac{\partial A_r}{\partial z} = 0$
CD	1 atm	$\frac{\partial u_z}{\partial r} = 0$	$\frac{\partial u_r}{\partial r} = 0$	1000	0	0	0
DE	1 atm	$\frac{\partial u_z}{\partial z} = 0$	$\frac{\partial u_r}{\partial z} = 0$	1000	0	0	0
EA	–	0	0	3500	0	$\frac{\partial A_z}{\partial z} = 0$	$\frac{\partial A_r}{\partial z} = 0$
AA'	–	0	0	3500	$\jmath_z(r)$	$\frac{\partial A_z}{\partial z} = 0$	$\frac{\partial A_r}{\partial z} = 0$

C.3.1 Comparison

The results of simulations using FLUENT model has been compared with simulations result in [61]. Figure C.2 represents temperature fields found by our FLUENT model. A general bell curve is observed similar to the results in [61]. Similar to the Air Plasmas, Argon Plasma transport and thermodynamic properties vary with temperature and pressure. Modeling Argon Plasma is not our main objective. Hence we

have approximated the variation in Argon Plasma properties by polynomial fit to the data given in [12] at 1 atm pressure. Because of this approximation temperature field values shown in C.2 do not match exactly to those in [61]. Obtaining similar bell curve is satisfactory enough to validate our FLUENT model.

Figure C.3 shows the variation in axial velocity component along the axis AB. Though there is no inlet flow (i.e. 0 inlet velocity), flow is induced due to effects of *Lorentz* forces. Comparison with [61] shows the agreement with the profile though it do not match exact quantitatively, because of approximation in properties of Argon Plasma.

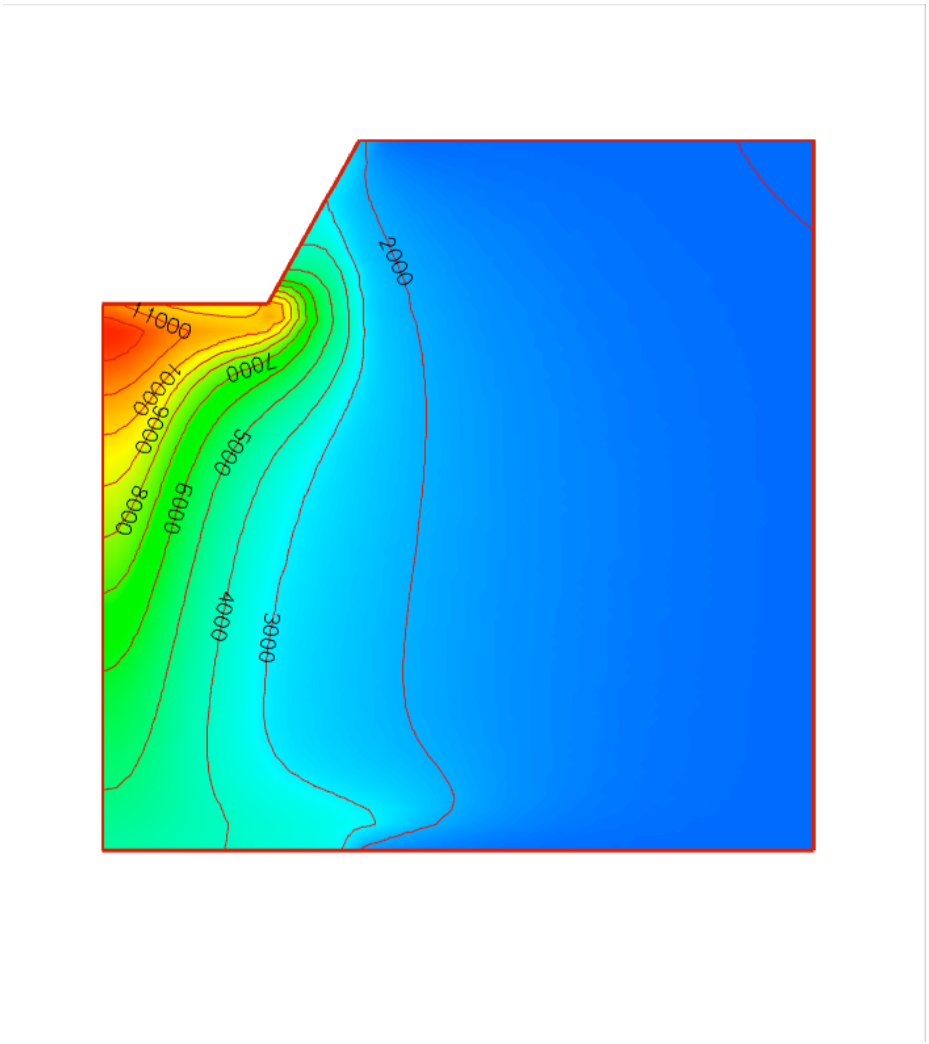

Figure C.2. Temperature(K) Fields.

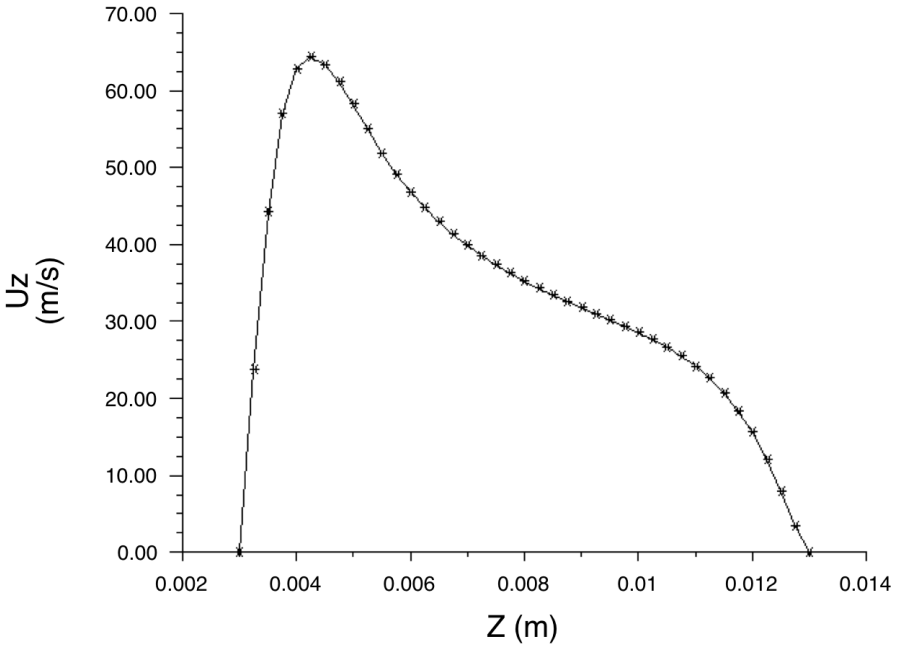

Figure C.3. Axial Velocity along the axis.